effectively using the conventional wide-pore column that was used for the FD–LC–MS/MS method. Therefore, we searched for other columns that have higher-performance separation ability than the wide-pore column.

According to recent technical developments, the use of a stationary phase of small and non-porous particles (sub-2 μm) reduces eddy diffusion and mass-transfer resistance in the mobile phase more than porous particles [8]. Chong et al. used sub-2 μm non-porous particles for separating intact proteins in biological samples [9]. However, the reproducibility of the retention time of each protein was very low, probably due to the hydrophobicity of the intact proteins and the large amount of proteins provided for ultraviolet detection, which could prevent using a non-porous column for differential proteomics analysis. In contrast, with FD–LC–MS/MS, the non-porous column seems to be useful because the proteins are derivatized into less hydrophobic ones with the hydrophilic reagent, and one or two orders of magnitude less amount of proteins is sufficient for fluorescence detection than for ultraviolet detection.

Therefore, in this study, we applied a non-porous small-particle reversed-phase column (Presto FF-C18, 2 μm particle, Imtakt) to the FD–LC–MS/MS method. Based on an investigation of column lengths and flow rates for the non-porous column, the optimized FD–LC–MS/MS method was applied to liver mitochondrial proteomics analysis, resulting in high-performance separation of the mitochondrial proteins. This result suggested the non-porous small-particle column as a replacement for the wide-pore column in differential proteomics analysis utilizing the FD–LC–MS/MS method. Also, the result of liver mitochondrial proteomics analysis indicated proteins related to hepatocarcinogenesis; thus, the roles of proteins in hepatocarcinogenesis will be investigated.

2. Experimental

2.1. Reagents

For this study, 7-chloro-N-[2-(dimethylamino)ethyl]-2,1,3-benzoxadiazole-4-sulfonamide (DAABD-Cl) and Buffer Solution pH 8.7 (6 M Guanidine Hydrochloride) were obtained from Tokyo Chemical Industry (Tokyo, Japan). In addition, 3-[(3-cholamidopropyl)dimethylammonio]propanesulfonate (CHAPS) and ethylenediamine-N,N,N′,N′-tetraacetic acid disodium salt (Na_2EDTA) were obtained from Dojindo Laboratories (Kumamoto, Japan). Tris(2-carboxyethyl)phosphine hydrochloride (TCEP) and β-lactoglobulin (M.W. 18,363) were purchased from Sigma–Aldrich (St. Louis, MO, USA). Calcitonin (M.W. 3,418) was purchased from Peptide Institute (Osaka, Japan). Trifluoroacetic acid (TFA) was obtained from Wako Pure Chemical Industries (Osaka, Japan). Acetonitrile (HPLC grade) was obtained from Kanto Chemical (Tokyo, Japan). All the other reagents were of analytical reagent grade and were used without further purification. Water was used after purification with the Milli-Q system (Nihon Millipore, Tokyo, Japan).

2.2. Columns

Non-porous spherical silica (2 μm particle and 2 m^2/g specific surface area) was utilized as packing material in the Presto FF-C18 column (Fig. 1) (Imtakt, Kyoto, Japan). Octadecylsilane (ODS) binds to functional groups on packing materials, indicating that Presto FF-C18 is useful for reversed-phase separation in HPLC. However, wide-pore spherical silica (30 nm pore size, 3 μm particle, and 100 m^2/g specific surface area) was utilized in the Intrada WP-RP column (Imtakt). Reversed-phase ligands exist on the surface of the packing materials of Intrada WP-RP, which was used as a conventional protein separation column for the FD–LC–MS/MS method. Presto FF-C18 columns were adopted with 4.6 mm i.d. and 50–250 mm length, while Intrada WP-RP with 4.6 mm i.d. and 250 mm length was usually utilized for protein separation [2–7].

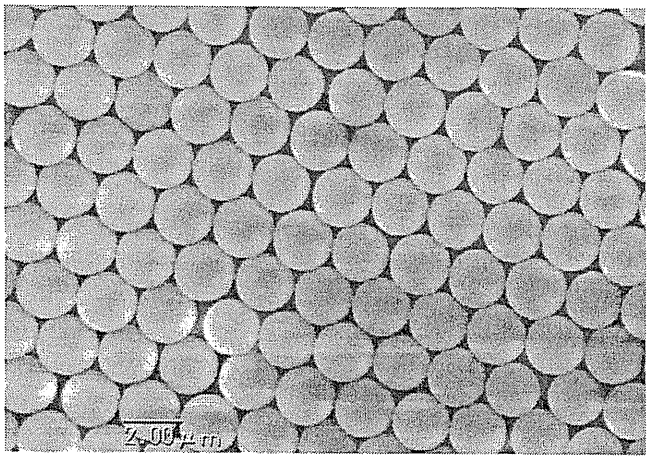

Fig. 1. Electron microscopic image of non-porous spherical silica (2 μm particle) utilized as a packing material in a Presto FF-C18 column.

2.3. FD reaction and separation of DAABD-calcitonin on the non-porous or the wide-pore column

A 10 μL aliquot of 5 μM calcitonin (Peptide Institute, Osaka, Japan) was mixed with 60 μL of 16.7 mM CHAPS/3.33 mM Na_2EDTA/0.833 mM TCEP in 6 M guanidine buffer (pH 8.7), 25 μL of 6 M guanidine buffer (pH 8.7), and 5.0 μL of 140 mM DAABD-Cl in acetonitrile. Each reaction mixture was incubated at 40 °C for 10 min, and the reaction was stopped with 3.0 μL of 20% TFAaq. The reaction mixture was then diluted threefold with the mobile phase. A 10 μL aliquot of the diluted reaction mixture was injected into an HPLC system that consisted of a pump (L-2100, Hitachi) and a fluorescence detector (L-2485, Hitachi). Fluorescence detection was carried out at 505 nm (excitation at 395 nm). Separation was performed on the non-porous column (4.6 i.d. × 50, 100, 150, or 250 mm) or the wide-pore column (4.6 i.d. × 250 mm) (Imtakt, Kyoto, Japan). The column temperature was set at 60 °C, and the flow rate was 0.2–0.5 mL/min. The gradient elution was 10–40% B over 60 min ((A) water:acetonitrile:TFA = 90:10:0.10, v/v/v; (B) water:acetonitrile:TFA = 30:70:0.20, v/v/v).

2.4. Preparation of liver mitochondrial sample and determination of total proteins

Sixteen-month-old Tg and NTg mice were used for analysis. Progression of disease state and morphological features were described in previous reports [4,10].

A preliminary study clearly indicated that an extraction procedure utilizing a mitochondrial isolation commercial kit was not useful, due to the low repeatability in isolation handling. Therefore, in this study, mitochondria were extracted from liver samples (100 mg) by density-gradient centrifugation using a mannitol/sucrose solution, as reported by Lopez et al. [11]. The mitochondrial pellet obtained was suspended with twice-volume of 2% CHAPS in 6 M guanidine buffer (pH 8.7). The suspension was sonicated for 15 s on ice four times at 15 s intervals. The sonicated suspension was centrifuged at 13,000 g for 2 min at 4 °C. The supernatant was then collected and stored as a soluble fraction at −80 °C after freezing with liquid nitrogen. The total liver mitochondrial proteins were determined with a BCA™ Protein Assay

Kit (Thermo Scientific, Rockford, IL, USA), following the written instructions. Bovine serum albumin was used as a protein standard.

2.5. FD–LC–MS/MS method for liver mitochondrial proteomics analysis

The previous method was used for the FD procedure for liver mitochondrial proteins with DAABD-Cl [4], except for the amount of total protein; in brief, 60 μg of liver mitochondrial proteins was derivatized in 100 μL reaction mixture. Twenty microliters of the reaction mixture (12 μg proteins) was subjected to HPLC. Sample proteins amount per injection was low enough as compared to the maximum (24 μg) for separation on the non-porous column. The overall system consisted of a Hitachi L-2000 series HPLC system with a non-porous column (4.6 i.d. × 250 mm) at a column temperature of 60 °C [2] and a flow rate of 0.3 mL/min. Fluorescence detection was carried out at 505 nm (excitation at 395 nm). The compositions of the mobile phases were the same as described above. The 267.5 min gradient program was used to compare the non-porous column with the wide-pore column. The gradient elution was 16% B held over 5 min, to 25% in 10 min, to 43% B in 112.5 min, to 45% B in 135 min, to 55% B in 185 min, to 65% B in 215 min, and to 100% B in 267.5 min. The 535 min gradient program was used for proteomics analysis of mitochondrial proteins in livers of the hepatitis-infected mouse model. The gradient elution was 16% B held over 10 min, to 25% in 20 min, to 43% B in 225 min, to 45% B in 270 min, to 55% B in 370 min, to 65% B in 430 min, and to 100% B in 535 min. To keep the long life-time of the non-porous column, a washing operation was performed after operation of each analysis. The gradient time program of the washing operation was 100 to 0% B in 5 min and 0 to 100% B in 10 min at 0.3 mL/min of flow rate, which was repeated four times.

The isolated derivatized proteins were identified as reported in Ref. [5] using HPLC and tandem mass spectrometry. The obtained amino acids sequence data were searched for the taxonomy *Mus musculus* against the National Center for Biotechnology Information non-redundant (NCBInr) database using MASCOT version 2.1.03 (Matrix Science, Ltd., London, UK).

3. Result

3.1. Separation of DAABD-calcitonin in gradient elution with the non-porous column

The non-porous column was applied to separate fluorogenic derivatized calcitonin, a model peptide, to investigate its separation efficiency. Calcitonin (0.5 μM, M.W. 3418) was derivatized with a fluorogenic reagent, 7.0 mM DAABD-Cl, and subjected to HPLC-fluorescence detection in gradient elution on either the non-porous or the wide-pore column. Both columns were the same size (4.6 i.d. × 250 mm). The retention times and shapes of both DAABD-calcitonin peaks suggested that the non-porous column exhibited stronger affinity for the peptide and higher resolution than the wide-pore column (Fig. 2). The retention time of the compounds less retained on the non-porous column was shorter than that on the wide-pore column. The separation efficiencies of both columns were then compared utilizing the peak capacity, since the separation efficiency of HPLC columns in gradient elution is usually evaluated with column peak capacity P, while under isocratic conditions it is evaluated with theoretical plates N. The peak capacity represents the maximum theoretical number of components that can be separated in a column within a given gradient time. Each P value was then calculated from peak width w measured at 4σ

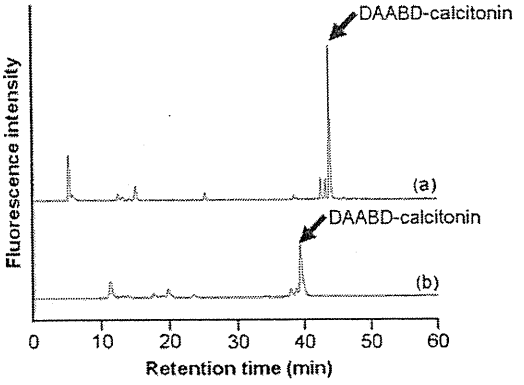

Fig. 2. Chromatograms obtained from DAABD-calcitonin separated in (a) the non-porous column or (b) the wide-pore column under gradient elution conditions. Chromatographic conditions are described in Section 2.

(13.4% of peak height) and the gradient time t_g according to Eq. (1) [12]:

$$P = 1 + \frac{t_g}{w} \quad (1)$$

The P value with the non-porous column was found to be three-fold higher than that with the wide-pore column under 60 min gradient conditions (197 with the non-porous column vs. 64 with the wide-pore column). In a similar experiment using a typical standard protein (β-lactoglobulin, M.W. 18,363), the P value exhibited the same tendency with both columns (data not shown). These results indicate that separation efficiency in the non-porous column was superior to that in the wide-pore column.

3.2. Optimized column length and flow rate with the non-porous column

In order to obtain appropriate separation efficiency, the gradient elution of DAABD-calcitonin was performed with different lengths (50, 100, 150, and 250 mm) of the non-porous column at different flow rates (0.2, 0.3, 0.4, and 0.5 mL/min). However, for the 250 mm-long column, the flow rate was limited to a maximum of 0.3 mL/min because of the durability of the HPLC flow (20 MPa) system used in the present experiment. DAABD-calcitonin was separated in the same 60 min gradient program as described in Section 3.1, and each P value was calculated according to Eq. (1). The P value increased with increasing column length and flow rate, indicating that separation efficiency was greater with a longer column and a higher flow rate (Fig. 3A). The same was true for β-lactoglobulin, a model protein (data not shown).

Moreover, mitochondrial protein extract was injected into each length of the columns at the maximum flow rate (0.3 or 0.5 mL/min) to investigate the separation of a real biological sample. The number of separated protein peaks increased with increasing column length: a 250 mm-long column at a 0.3 mL/min flow rate exhibited the highest separation efficiency for the actual protein mixture sample (Fig. 3B). Therefore, a column length of 250 mm with a flow rate of 0.3 mL/min was selected for separating the mitochondrial protein extract.

3.3. Comparison of the non-porous column with the wide-pore column for separating a mitochondrial protein extract

Based on the results above, the non-porous column (250 mm length with a flow rate of 0.3 mL/min) was applied to separate a mitochondrial protein extract. The chromatogram obtained under the appropriate conditions described in Section 2.5 was compared with that obtained from the wide-pore column (250 mm length,

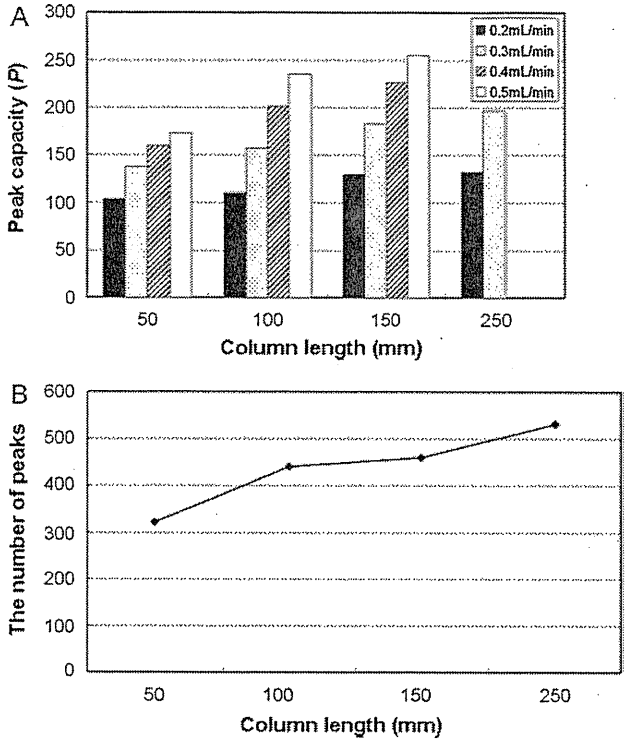

Fig. 3. (A) Peak capacities of the non-porous column with various column lengths (50, 100, 150, and 250 mm) at various flow rates (0.2, 0.3, 0.4, and 0.5 mL/min) in the gradient elution of DAABD-calcitonin. Each *P* value was calculated with Eq. (1) in Section 3.2. (B) The number of protein peaks separated in each length of the column (50, 100, 150, and 250 mm) obtained from the mitochondrial protein extract. The flow rate was 0.5 mL/min, except for the 250 mm column that had a 0.3 mL/min flow rate. The details are described in Section 2.

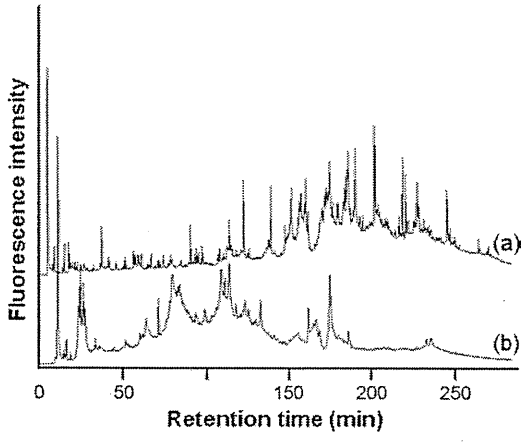

Fig. 4. Chromatograms of mouse liver mitochondrial proteins separated in (a) the non-porous column or (b) the wide-pore column. Chromatographic conditions are described in Section 2.

0.3 mL/min). Fig. 4a indicates that 420 protein peaks were obtained on the chromatogram with the non-porous column in 260 min analytical time. However, 160 protein peaks were not clearly separated in the chromatogram with the wide-pore column (Fig. 4b). This result clearly suggested that the non-porous column, rather than the wide-pore column, would be useful for proteomics analysis of mouse liver mitochondrial proteins with the FD–LC–MS/MS method.

Also, the retention times and peak shapes of the proteins injected into the non-porous column exhibited stronger adsorption and higher resolution than those injected into the wide-pore column. Furthermore, the retention time of the compounds less

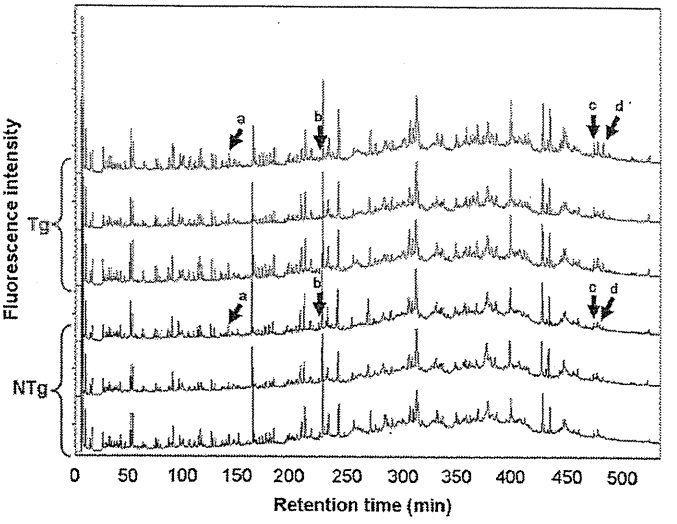

Fig. 5. Chromatograms of liver mitochondrial proteins in Tgs (red) and NTgs (blue) mice separated in the non-porous column. The peaks indicated by arrows fluctuated between Tgs and NTgs. Chromatographic conditions are described in Section 2. (For interpretation of the references to color in this figure legend, the reader is referred to the web version of the article.)

retained in the non-porous column was shorter than that on the wide-pore column.

3.4. Proteomics analysis of mitochondrial proteins in livers of hepatitis-infected mouse model

Differential proteomics analysis was performed on the non-porous column between mitochondrial protein samples extracted from livers of Tgs ($n=3$) and NTgs ($n=3$) mice aged 16 months. This age was selected based on the previous report that many proteins related to the function of mitochondrial events fluctuated in Tg. The appropriate separation conditions in HPLC afforded 500 protein peaks on each chromatogram for Tgs and NTgs in 9 h of analysis (Fig. 5), with each peak height representing the amount of each protein. The responsibility of this analysis was confirmed, based on the reproducibility of the retention times and the peak heights. The relative standard deviations (RSDs) of peaks a through d (Fig. 5) ranged from 0.0 to 0.5% for retention times and 0.4–18.0% for peak heights (for between-days, $n=3$–6). The heights of peaks corresponding to specific retention times were compared between Tgs and NTgs. The expression of several peaks fluctuated, and each fluctuating peak fraction was collected, digested, and subjected to LC–MS/MS analysis to identify the protein. Table 1 summarizes the identified proteins. Three proteins were significantly up-regulated ($Tg/NTg = 1.24$–2.86, $0.05 \leq p < 0.10$) (Peaks a, c, and d in Fig. 5) in Tg, while one protein peak was significantly down-regulated ($Tg/NTg = 0.44$, $p < 0.05$) (Peak b in Fig. 5). Those four proteins were demonstrated for the first time in liver mitochondrial proteomics analysis.

4. Discussion

4.1. Comparison of the separation of DAABD-calcitonin and DAABD-β-lactoglobulin between the non-porous column and the wide-pore column

In order to determine the difference in separation between the non-porous column and the wide-pore column, a derivatized model peptide and protein (DAABD-calcitonin and DAABD-β-lactoglobulin) were separated. The retention times of the derivatized model samples were longer for the non-porous col-

Table 1
Differentially expressed liver mitochondrial proteins between Tgs and NTgs.

Peak number	Tg/NTg ratio		Protein name	Accession number	Score	Sequence coverage (%)
a	1.24	± 0.17	60S ribosomal protein L11	gi 13385408	129	12
b	0.44	± 0.33	Sterol-carrier protein 2	gi 45476581	278	10
c	1.51	± 0.35	NADH-cytochrome b5 reductase 3	gi 19745150	145	8
d	2.86	± 1.30	Hydroxysteroid (17-beta) dehydrogenase 13	gi 159573879	183	25

umn than for the wide-pore column. Since the surface of the non-porous column is covered with ODS (C18) and the surface of the wide-pore column consists of a less hydrophobic "reversed-phase" ligand than C18, stronger retention of the derivatized model samples should be caused by the hydrophobic interaction in the non-porous column. In contrast, considering the shortest retention times of the hydrophilic substances, the non-porous column should exhibit fewer void volumes than the wide-pore column. It was also shown that, considering the *P* (peak capacity) value for the non-porous column was threefold higher than that for the wide-pore column, the non-porous and small size (2 μm as compared to 3 μm of the wide-pore column) reduced eddy diffusion and mass-transfer resistance on separation and resulted in high-resolution chromatography [8]. This couldn't be caused by the narrow particle size distribution of the former column since the particle size distribution of both the columns were similar (D90/D10 < 1.4, and D90/D10 = 1.42 for the non-porous and the wide-pore, respectively, measured by laser diffraction particle size analysis and electrical sensing zone method).

4.2. Optimization of column length and flow rate for protein separation with the non-porous column

The effects of column length and flow rate on the *P* value were investigated using DAABD-calcitonin and DAABD-β-lactoglobulin to obtain optimal conditions for derivatized protein separation on the non-porous column. High *P* values were obtained using a longer column and a higher flow rate. This tendency agreed with the simulation of separation efficiency reported by Gilar et al. [12], indicating that the length of the non-porous column was proportional to separation efficiency. In this study, 0.3 mL/min was the maximum flow rate for the longest column (250 mm) because of the currently limited operating pressure (20 MPa). The LC system should be mechanically strong enough to withstand the ultrahigh pressures for further efficient separation in the non-porous Presto FF-C18 that might be 250 mm long and have a flow rate exceeding 0.3 mL/min. In this sense, in the future, further efficient separation should be examined utilizing an Ultra High Pressure Liquid Chromatography system. According to the results (Fig. 3A), the highest *P* value was obtained with a 150 mm length of column and a flow rate of 0.5 mL/min. However, more separated proteins were observed in the 250 mm-long column with a 0.3 mL/min flow rate for the mitochondrial sample (Fig. 3B). This is because the separable peaks from a large numbers of proteins in a real biological sample should be proportional to the column length. Another reason is that the dilution of the peak fraction in a 150 mm column with a high flow rate of 0.5 mL/min might be beyond the detection limit of the system. Therefore, a 250 mm column length with a flow rate of 0.3 mL/min was adopted as the optimal condition for separating liver mitochondrial proteins.

4.3. Application of the FD–LC–MS/MS method using the non-porous column for differential proteomics analysis of liver mitochondria

Nine hours of analysis indicated that the number (500) of mitochondrial protein peaks (Fig. 5) was similar to the number of extracted proteins from a whole cell separated with the wide-pore column (e.g., for mouse liver proteomics analysis) [4]. Concerning the life-time of the non-porous column, the life-time was long enough to analyze mitochondrial proteins about 40 times (400 h including the washing period) since the chromatogram obtained after 40 times analyses was the same as the initial one. That would be caused by the contribution of a washing operation after each analysis. This result suggests that the non-porous column could be substituted for the wide-pore column as a protein separation column for the FD–LC–MS/MS method.

Compared to the low reproducibility for the retention times of peaks in the previous report [9], the present differential proteomics analysis of liver mitochondria obtained reproducible retention times and peak heights (RSD less than 0.5% for retention times and less than 18.0% for peak heights). The reason for this superior reproducibility may be that in the FD–LC–MS/MS method, proteins were derivatized with the hydrophilic reagent and a low amount of proteins. These results indicate that the FD–LC–MS/MS method using the non-porous column can be used for differential proteomics analysis of liver mitochondria and results in identification of four fluctuating proteins between Tgs and NTgs.

4.4. Functions of the fluctuating liver mitochondrial proteins related to hepatocarcinogenesis

All the identified mitochondrial proteins in this study were demonstrated for the first time in liver proteomics analysis. Since mitochondria were extracted from mouse liver and analyzed for expression of proteins, it is assumed that the proteins inside the mitochondria were concentrated to a detectable level of each expression fluctuation.

Only one down-regulated peak in Tg was identified as sterol carrier protein 2 (SCP2), considering differences in localization between the deduced different types (SCP2 and SCPx) (reviewed in ref. [13]). SCP2 is related to intracellular lipid transport (e.g., cholesterol) from other intracellular membranes to mitochondria [14], as well as from the outer to the inner mitochondrial membrane for oxidation. Since lipids have accumulated in the hepatocytes of 16-month-old Tg mice, causing steatosis as previously reported [10], lipid transport to mitochondria might no longer be required. Thus, SCP2 was decreased in Tg through a negative feedback pathway. Also, SCP2 is reportedly involved in regulation of the signal pathway for lipids (reviewed in ref. [13]). These findings suggest that the decrease of SCP2 in Tg may suppress lipid transport to mitochondria, leading to inhibition of lipid signaling. In contrast, three proteins were demonstrated to be up-regulated in Tg. Hydroxysteroid (17-beta) dehydrogenase 13 (17βHSD13) is specifically expressed in liver [15]. It has been reported that the intracellular localization of 17βHSD13 is similar to that of HCV core protein in endoplasmic reticulum (ER), lipid droplets (LDs), and mitochondria [16–18], while it is unknown whether 17βHSD13 localizes in mitochondria or not. In general, 17βHSD family proteins catalyze the dehydrogenation reactions of the steroid skeleton with an excess of NADH or electrons. Although 17βHSD13 may play a key role in the next step of detoxification and/or utilization of lipid metabolites through the reaction, its specific substrate is not identified. At least, the increase of 17βHSD13 in Tgs would acti-

vate lipid metabolism. NADH-cytochrome b5 reductase 3 (CYB5R3) was observed in the plasma membrane, mitochondrial outer membrane, and ER. CYB5R3 in the mitochondrial electron-transfer system catalyzes the oxidation of NADH to NAD^+ (reviewed in Ref. [19]). For mitochondrial dysfunction, CYB5R3 is up-regulated due to an increase of the NADH/NAD^+ ratio, resulting in enhanced oxidation of NADH to NAD^+. Thus, an increase of CYB5R3 in Tg would accelerate aerobic respiration in mitochondria. In addition, 60S ribosomal protein L11 (RPL11) is associated with Mdm2, which is an E3 ligase for promoting p53 ubiquitination, resulting in prevention of the degradation of p53 [20,21]. The undegraded p53 in mitochondria reportedly causes apoptosis of cancer cells [22,23]. This finding suggests that up-regulated RPL11 would suppress the growth of hepatocarcinoma in transition out of hepatitis C. If hepatocarcinogenesis activates metabolism in Tg mice at the age of 16 months, 17βHSD13 and CYB5R3 might increase and accelerate lipid metabolism and aerobic respiration. Furthermore, a decrease of SCP2 might control lipid transport to mitochondria and thus maintain equilibrium through a negative feedback pathway. Considering these results, fluctuation of these proteins suggests that activation and suppression of hepatocarcinogenesis occur simultaneously in Tg mice at 16 months of age.

In conclusion, a novel non-porous column (Presto FF-C18) achieved good separation of liver mitochondrial proteins, which was hardly achieved on a wide-pore column such as Intrada WP-RP. Moreover, the FD–LC–MS/MS method with Presto FF-C18 demonstrated for the first time several fluctuating proteins performing differential proteomics analysis of liver mitochondrial proteins in a hepatitis-infected mouse model.

References

[1] H.J. Issaq, J. Blonder (Eds.), J. Chromatogr. B: Analyt. Technol. Biomed. Life Sci. Netherlands (2009) 1222.
[2] M. Masuda, H. Saimaru, N. Takamura, K. Imai, Biomed. Chromatogr. 19 (2005) 556.
[3] T. Ichibangase, H. Saimaru, N. Takamura, T. Kuwahara, A. Koyama, T. Iwatsubo, K. Imai, Biomed. Chromatogr. 22 (2008) 232.
[4] T. Ichibangase, K. Moriya, K. Koike, K. Imai, J. Proteome Res. 6 (2007) 2841.
[5] K. Imai, T. Ichibangase, R. Saitoh, Y. Hoshikawa, Biomed. Chromatogr. 22 (2008) 1304.
[6] H. Asamoto, T. Ichibangase, K. Uchikura, K. Imai, J. Chromatogr. A 1208 (2008) 147.
[7] T. Ichibangase, K. Imai, J. Proteome Res. 8 (2009) 2129.
[8] N. Wu, Y. Liu, M.L. Lee, J Chromatogr A, Netherlands (2006) 142.
[9] B.E. Chong, D.M. Lubman, F.R. Miller, A.J. Rosenspire, Rapid Commun. Mass Spectrom. 13 (1999) 1808.
[10] K. Moriya, H. Yotsuyanagi, Y. Shintani, H. Fujie, K. Ishibashi, Y. Matsuura, T. Miyamura, K. Koike, J. Gen. Virol. 78 (Pt 7) (1997) 1527.
[11] M.F. Lopez, B.S. Kristal, E. Chernokalskaya, A. Lazarev, A.I. Shestopalov, A. Bogdanova, M. Robinson, Electrophoresis 21 (2000) 3427.
[12] M. Gilar, A.E. Daly, M. Kele, U.D. Neue, J.C. Gebler, J. Chromatogr. A 1061 (2004) 183.
[13] F. Schroeder, B.P. Atshaves, A.L. McIntosh, A.M. Gallegos, S.M. Storey, R.D. Parr, J.R. Jefferson, J.M. Ball, A.B. Kier, Biochimica Et Biophysica Acta-Mol. Cell Biol. Lipids 1771 (2007) 700.
[14] G.G. Martin, H.A. Hostetler, A.L. McIntosh, S.E. Tichy, B.J. Williams, D.H. Russell, J.M. Berg, T.A. Spencer, J. Ball, A.B. Kier, F. Schroeder, Biochemistry 47 (2008) 5915.
[15] Y. Horiguchi, M. Araki, K. Motojima, Biochem. Biophys. Res. Commun. 370 (2008) 235.
[16] K. Moriya, H. Fujie, Y. Shintani, H. Yotsuyanagi, T. Tsutsumi, K. Ishibashi, Y. Matsuura, S. Kimura, T. Miyamura, K. Koike, Nat. Med. 4 (1998) 1065.
[17] R. Suzuki, S. Sakamoto, T. Tsutsumi, A. Rikimaru, K. Tanaka, T. Shimoike, K. Moriishi, T. Iwasaki, K. Mizumoto, Y. Matsuura, T. Miyamura, T. Suzuki, J. Virol. 79 (2005) 1271.
[18] B. Schwer, S.T. Ren, T. Pietschmann, J. Kartenbeck, K. Kaehlcke, R. Bartenschlager, T.S.B. Yen, M. Ott, J. Virol. 78 (2004) 7958.
[19] R. de Cabo, E. Siendones, R. Minor, P. Navas, Aging (Albany NY) 2 (2010) 63.
[20] K. Itahana, H. Mao, A.W. Jin, Y. Itahana, H.V. Clegg, M.S. Lindstrom, K.P. Bhat, V.L. Godfrey, G.I. Evan, Y.P. Zhang, Cancer Cell 12 (2007) 355.
[21] S. Fumagalli, A. Di Cara, A. Neb-Gulati, F. Natt, S. Schwemberger, J. Hall, G.F. Babcock, R. Bernardi, P.P. Pandolfi, G. Thomas, Nat. Cell Biol. 11 (2009) 501.
[22] N.D. Marchenko, A. Zaika, U.M. Moll, J. Biol. Chem. 275 (2000) 16202.
[23] M. Mihara, S. Erster, A. Zaika, O. Petrenko, T. Chittenden, P. Pancoska, U.M. Moll, Mol. Cell 11 (2003) 577.

Research Article

EASL EUROPEAN ASSOCIATION FOR THE STUDY OF THE LIVER | JOURNAL OF HEPATOLOGY

Pathogenesis of lipid metabolism disorder in hepatitis C: Polyunsaturated fatty acids counteract lipid alterations induced by the core protein

Hideyuki Miyoshi[1], Kyoji Moriya[1], Takeya Tsutsumi[1], Seiko Shinzawa[1], Hajime Fujie[1], Yoshizumi Shintani[1], Hidetake Fujinaga[1], Koji Goto[1], Toru Todoroki[2], Tetsuro Suzuki[3], Tatsuo Miyamura[3], Yoshiharu Matsuura[4], Hiroshi Yotsuyanagi[1], Kazuhiko Koike[1,*]

[1]*Department of Internal Medicine, Graduate School of Medicine, University of Tokyo, Tokyo, Japan;* [2]*Department of Laboratory Medicine, Keio University School of Medicine, Tokyo, Japan;* [3]*Department of Virology II, National Institute of Infectious Diseases, Tokyo, Japan;* [4]*Department of Molecular Virology, Research Institute for Microbial Diseases, Osaka University, Osaka, Japan*

Background & Aims: Disturbance in lipid metabolism is one of the features of chronic hepatitis C, being a crucial determinant of the progression of liver fibrosis. Experimental studies have revealed that the core protein of hepatitis C virus (HCV) induces steatosis.

Methods: The activities of fatty acid metabolizing enzymes were determined by analyzing the fatty acid compositions in HepG2 cells with or without core protein expression.

Results: There was a marked accumulation of triglycerides in core-expressing HepG2 cells. While the oleic/stearic acid (18:1/18:0) and palmitoleic/palmitic acid ratio (16:1/16:0) were comparable in both the core-expressing and the control cells, there was a marked accumulation of downstream product, 5,8,11-eicosatrienoic acid (20:3(n-9)) in the core-expressing HepG2 cells. The addition of eicosatetraynoic acid, which inhibits delta-6 desaturase activity which is inherently high in HepG2 cells, led to a marked accumulation of oleic and palmitoleic acids in the core-expressing cells, showing that delta-9 desaturase was activated by the core protein. Eicosapentaenoic acid (20:5(n-3)) or arachidonic acid (20:4(n-6)) administration significantly decreased delta-9 desaturase activity, the concentration of 20:3(n-9), and triglyceride accumulation. This lipid metabolism disorder was associated with NADH accumulation due to mitochondrial dysfunction, and was reversed by the addition of pyruvate through NADH utilization.

Conclusions: The fatty acid enzyme, delta-9 desaturase, was activated by HCV core protein and polyunsaturated fatty acids counteracted this impact of the core protein on lipid metabolism. These results may open up new insights into the mechanism of lipid metabolism disorder associated with HCV infection and provide clues for the development of new therapeutic devices.

Keywords: Steatosis; Oleic acid; Core protein; Lipid metabolism; Desaturase; Hepatocellular carcinoma; NADH.

Received 31 March 2010; received in revised form 8 June 2010; accepted 5 July 2010; available online 22 September 2010

* Corresponding author. Address: Department of Gastroenterology, Graduate School of Medicine, University of Tokyo, 7-3-1 Hongo, Bunkyo-ku, Tokyo 113-8655, Japan. Tel.: +81 3 5800 8800; fax: +81 3 5800 8799.

E-mail address: kkoike-tky@umin.ac.jp (K. Koike).

Abbreviations: HCV, hepatitis C virus; HCC, hepatocellular carcinoma; PUFA, polyunsaturated fatty acids; PPAR, peroxisome proliferators-activated receptors; SREBP, sterol regulatory element binding protein; EPA, eicosapentaenoic acid; AA, arachidonic acid; ETYA, eicosatetraynoic acid; NADH, nicotinamide adenine dinucleotide; KBR, ketone body ratio.

Introduction

Persistent hepatitis C virus (HCV) infection leads to the development of chronic hepatitis, cirrhosis, and eventually, hepatocellular carcinoma (HCC), thereby being a serious problem worldwide both in medical and in socio-economical settings [1]. Histologically, several distinct features, such as bile duct damage, lymphoid follicle formation, and steatosis, (fatty change) characterize chronic hepatitis C [2–4]. Among these, steatosis is reproducible in experimental systems, both *in vitro* and *in vivo*, in which HCV proteins, particularly the core protein of HCV, are expressed. The introduced core gene induces the formation of lipid droplets in the cytoplasm of cultured cells [5,6], and in transgenic mice, it induces hepatic steatosis resembling that in chronic hepatitis C patients [7–10].

In addition, evidence has accumulated showing that steatosis is a crucial determining factor for the progression of liver fibrosis [11–13]. Steatosis and serum lipid profiles are also associated with sustained virological response to ribavirin/interferon combination therapy [14,15]. Moreover, HCV transgenic mice resemble chronic hepatitis C patients in terms of the development of HCC, implying that the HCV core protein is one of the most important viral molecules in the pathogenesis of hepatitis C [16,17]. It would thus be meaningful to explore the precise role of the core protein in modulating lipid metabolism, which may also be involved in hepatocarcinogenesis. More recently, involvement of the metabolism of lipids such as sphingolipids or cholesterol has been implicated in the replication of HCV, with a formation of lipid rafts, which are considered to be the place for HCV replication [18,19], hereby highlighting again the importance of lipid metabolism in HCV infection.

ELSEVIER

Journal of Hepatology **2011** vol. 54 | 432–438

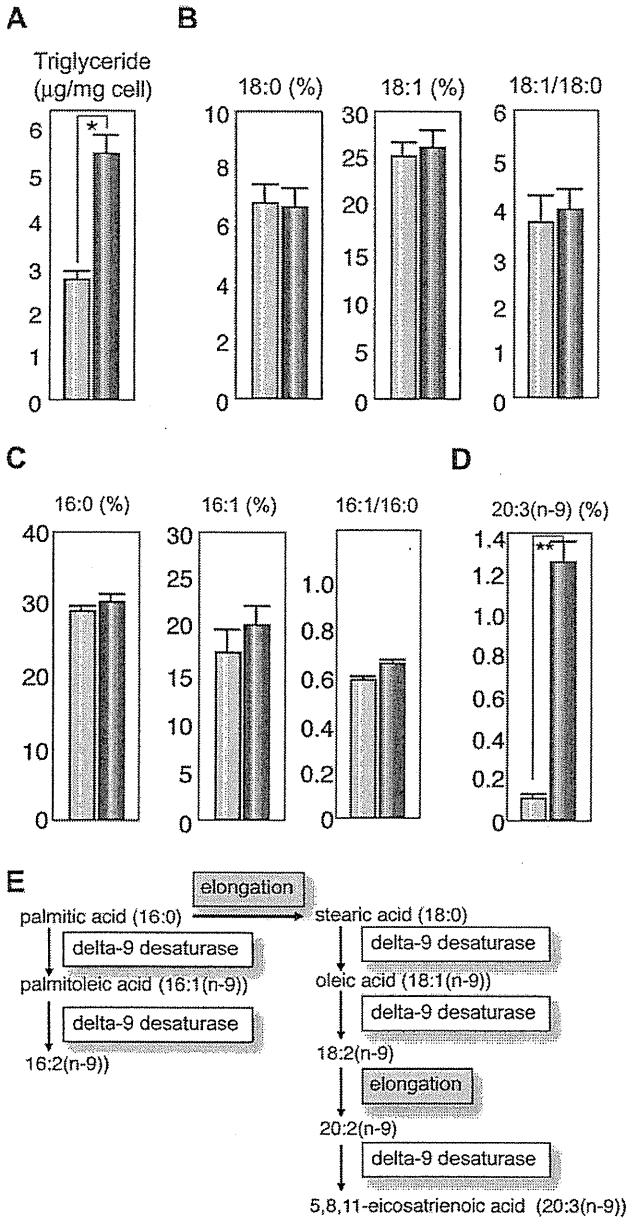

Fig. 1. Effect of the core protein on fatty acid composition in HepG2 cells. The fatty acid compositions of the total cell lipids were analyzed and the ratios of 18:1/18:0 and 16:1/16:0 in the core-expressing and control HepG2 cells were calculated. (A) Concentrations of triglycerides. (B) Percentages of stearic acid (18:0) and oleic acid (18:1(n-9)), and the 18:1/18:0 ratio. (C) Percentages of palmitic acid (16:0) and palmitoleic acid (16:1(n-9)), and the 16:1/16:0 ratio. (D) Percentage of eicosatrienoic acid (20:3(n-9). (E) Schematic display of synthetic pathway of n-9 fatty acids. Light blue bars indicate control cells and dark blue bars indicate core-expressing cells. Values represent the mean ± SE, $n = 5$ in each group. $^{*}p < 0.05$, $^{**}p < 0.01$.

Previously, we reported that the concentration of oleic acid (18:1(n-9)) was increased compared with that of stearic acid (18:0) in liver tissues of chronic hepatitis C patients as well as in those of mice transgenic for the HCV core gene [8]. Such a change may lead to increased membrane fluidity, owing to the lower melting temperature of monounsaturated fatty acids, resulting in incremental metabolism and proliferation of hepatocytes [20–22]. On the other hand, polyunsaturated fatty acids (PUFAs), such as eicosapentaenoic acid (20:5(n-3)) and arachidonic acid (20:4(n-6)), are known to activate the nuclear transcription of peroxisome proliferator-activated receptors (PPAR) and suppress the sterol regulatory element binding protein (SREBP)-1. While PPARγ induces delta-9 desaturase (stearoyl-CoA desaturase) gene expression, PUFAs suppresses delta-9 desaturase activity [23]. In the current study, we determined fatty acid desaturase activities by analyzing the fatty acid compositions in HepG2 cells expressing HCV core protein by chromatography. In addition, we determined whether exogenous PUFAs restore HCV-associated changes in fatty acid metabolism.

Materials and methods

Reagents

Eicosapentaenoic acid (EPA), arachidonic acid (AA), and eicosatetraynoic acid (ETYA) were purchased from Sigma Chemical (St. Louis, MO). Other chemicals were of analytical grade and purchased from Wako Chemicals (Tokyo, Japan).

Cell culture

This study was performed using HepG2 cell lines expressing the HCV core protein under the control of the CAG promoter (Hep39J, Hep396 and Hep397), or a control HepG2 line (Hepswx) carrying an empty vector, which were described previously [24], and control bulk HepG2 cells. They were maintained in Dulbecco's modified Eagle's medium (DMEM), supplemented with 10% fetal bovine serum (Invitrogen), 1 mg/ml G418, 100 U/ml penicillin, and 100 μg/ml streptomycin in a humidified atmosphere at 37 °C in 5% CO_2. Fatty acids were dissolved in DMEM containing defatted bovine serum albumin. The ratio of fatty acids to albumin (mole/mole) was 0.7. The cells were exposed to fatty acid–albumin complexes at various concentrations for 48 h. All the experiments were repeated at least five times.

Lipid extraction, measurement of triglyceride content, and analysis of fatty acid composition

Total cell lipids were extracted by Foch's method. The cells were washed twice with phosphate-buffered saline and collected by centrifugation. The cell pellets were homogenized with 10 vole of chloroform: methanol solution (2:1), and the mixture was shaken for 5 min. The lower phase was then washed with 4 vole of saline, dried on anhydrous sodium sulfate, and evaporated to complete dryness. For the analysis of fatty acid composition, the residue was methanolysed by the modified Morrison and Smith method with boron trifluoride as a catalyst [25]. Fatty acid methyl esters were analyzed using a Shimadzu GC-7A gas chromatograph (Shimadzu Corp., Kyoto, Japan).

Measurement of the ketone body ratio and lactate/pyruvate

The cells were cultured to confluence on 3.5 cm dishes, and the medium was replaced with 700 μl of fresh one. After 24 h of incubation, the levels of acetoacetate and β-hydroxybutyrate in the medium were measured by monitoring the production or consumption of nicotinamide adenine dinucleotide (NADH) with Ketorex kit (Sanwa Chemical, Nagoya, Japan) [26]. The ketone body ratio (KBR) was calculated as the acetoacetate/β-hydroxybutyrate ratio. The lactate and pyruvate levels in the medium were measured at random times by the lactate oxidase method and pyruvate oxidase method, respectively.

Effect of pyruvate on lipid metabolism

In some experiments, pyruvate (Wako Chemicals) was added to culture medium at a final concentration of 0, 1, 5, or 10 mM. After 48 h of incubation at 37 °C, the cells were harvested and subjected to fatty acid composition analysis or real-time PCR analysis.

Real-time PCR

RNA was prepared from cultured cells using TRIzol LS (Invitrogen, Carlsbad, CA). The fluorescent signal was measured using ABI prism 7000 (Applied Biosystems, Tokyo, Japan). The genes encoding mouse sterol regulatory element-binding proteins (SREBP)-1a, SREBP-1c, delta-9 desaturase, and hypoxanthine phosphoribosyltransferase were amplified with the primer pairs CACAGCGGTTTTGAACGAC and CTGGCTCCTCTTTGATCCCA, ACGGAGCCATGGATTGCACATTTG and TACATCTT TAAAGCAGCGGGTGCCGATGGT, TTCCCTCCTGCAAGCTCTAC and CGCAAGAAGG TGCTAACGAAC, and CCAGCAAGCTTGCAACCTTAACCA and GTAATGATCAGTCAAC GGGGGAC, respectively.

Statistical analysis

Data are presented as the mean ± SE. The data were analyzed by Mann–Whitney *U* test. Differences were considered statistically significant when $p < 0.05$.

Results

Triglyceride content in HepG2 cells expressing HCV core protein

To validate the relationship between the lipid accumulation and the core protein, we first determined the triglyceride contents in core-protein-expressing HepG2 clones (core-expressing cells), Hep39J, Hep396, Hep397, and control HepG2 cells. Core-expressing Hep396 cells contained significantly larger amounts of triglyceride than the control cells (Fig. 1A, $p < 0.01$), which are consistent with the results of previous studies on culture cells and transgenic mice [6,7,27]. Similar results were obtained with the other core-expressing cell lines.

Fatty acid compositions of total cell lipids

Analysis on the fatty acid compositions of total lipids revealed that the concentration of oleic acid (18:1(n-9)) and the ratio of oleic acid/stearic acid (18:1/18:0) in the core-expressing cells are similar to those in the control cells (Fig. 1B). The ratio of palmitoleic acid (16:1(n-9))/palmitic acid (16:1/16:0) was higher in the core-expressing cells than that in the control cells, but the difference was not significant (Fig. 1C). This rather dissociates from the results obtained in HCV core gene transgenic mice, in which the 18:1/18:0 ratio was significantly higher than that in control mice, thereby suggesting an increased delta-9 desaturase activity as a consequence of the HCV core protein expression [8]. However, it should be noted that the concentration of 5,8,11-eicosatrienoic acid (20:3(n-9)), a downstream product of n-9 fatty acid desaturation, was approximately13 times higher in the core-expressing cells than that in the control cells (Fig. 1D and E, $p < 0.01$). This is due to the fact that the activity of the delta-6 desaturase, an enzyme downstream of delta-9 desaturase, is also high in HepG2 cells, resulting in the relatively lower concentration of 18:1 in the core-expressing cells despite the high delta-9 desaturase activity. Actually, the delta-6 desaturase activity has been shown to be inherently high in HepG2 cells [28,29].

To verify this possibility, we administered ETYA, which inhibits delta-6 desaturase activity, to the cell cultures. Because similar results were obtained with the other core-expressing HepG2 cell lines, subsequent experiments were carried out using the Hep396 cell line. The addition caused significant increases in both 18:1/18:0 and 16:1/16:0 ratios in the core-expressing cells but not in the control cells (Fig. 2A 0 vs. 10 μg/ml and 0 vs. 50 μg/ml; $p < 0.05$, respectively). When compared between the

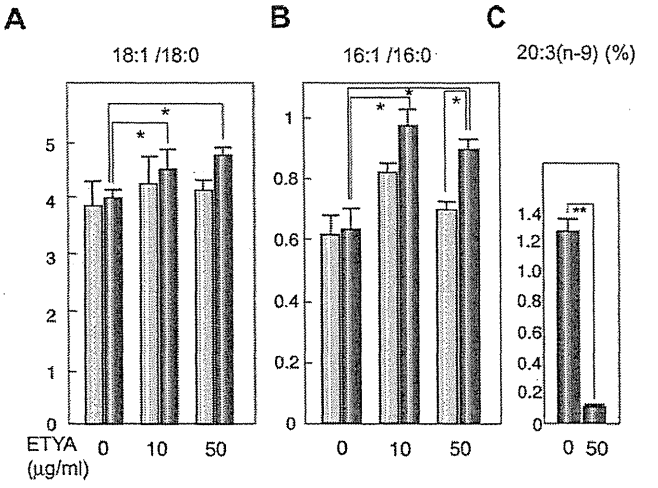

Fig. 2. Effect of ETYA on delta-9 desaturase index. HepG2 cells with or without the core protein were incubated with ETYA for 48 h. The fatty acid compositions of the total cell lipids were analyzed, and the ratios of 18:1/18:0 (A) and 16:1/16:0 (B), and the percentage of eicosatrienoic acid (20:3(n-9) (C) were computed. Light blue bars indicate control cells and dark blue bars indicate core-expressing cells. $N = 5$ in each group. *$p < 0.05$. ETYA, eicosatetraynoic acid.

core-expressing cells and control cells after the treatment with 50 μg/ml ETYA, the 18:1/18:0 ratio was higher and the 16:1/16:0 ratio was significantly higher (Fig. 2B, $p < 0.05$) in the core-expressing cells. ETYA (50 μg/ml) significantly decreased the concentration of 20:3(n-9) in the core-expressing cells (Fig. 2C, $p < 0.01$). These results suggest that the HCV core protein enhances the activities of delta-9, and possibly, delta-5 desaturases, modulating fatty acid metabolism in HepG2 cells, in which the delta-6 desaturase activity is intrinsically high (Fig. 1E) [28,29].

PUFAs modify fatty acid compositions and decrease triglyceride contents in HepG2 Cells

PUFAs are known to suppress the activities of both delta-9 and delta-6 desaturases. We, therefore, added PUFA, EPA, or AA, to the culture cell medium to examine the effect of PUFAs on the fatty acid compositions in HepG2 cells expressing the core protein. EPA and AA individually decreased the 18:1/18:0 and 16:1/16:0 ratios in a similar extent in both the core-expressing cells and the control cells (Fig. 3, $p < 0.05$). EPA and AA also significantly decreased the concentration of 20:3(n-9) in the core-expressing cells in a dose-dependent manner (Fig. 4, $p < 0.05$). In addition, EPA and AA individually decreased the triglyceride concentration in cells, in particular, in the core-expressing cells (Fig. 5, in core-expressing cells, $p < 0.01$; in control cells, $p < 0.05$, respectively).

Ketone body ratio and lactate/pyruvate ratio

Although the mechanism by which the HCV core protein enhances fatty acid desaturation is yet unclear, one possibility is the creation of an overreduced state in the core-expressing cells. The overreduced state or the accumulation of NADH in cells is known to accelerate the activities of fatty acid desaturases [30,31]. Such a condition may originate from the dysfunction of the mitochondrial electron transfer system (ETS), which has been

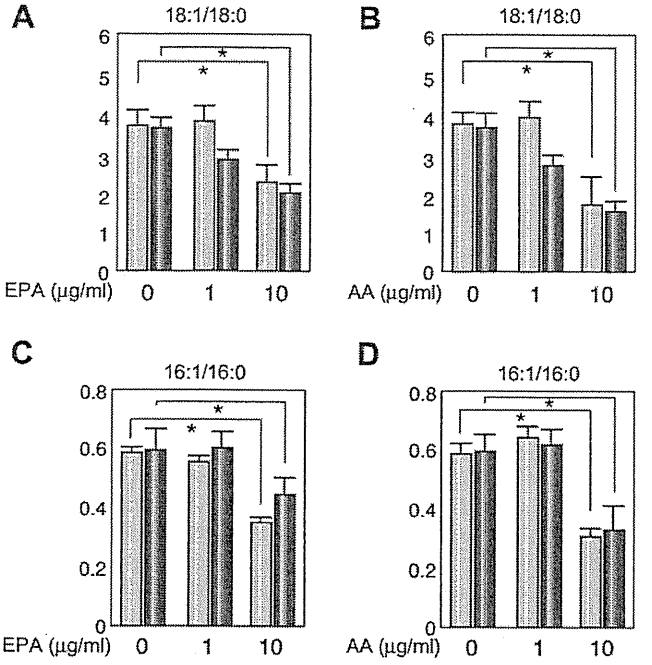

Fig. 3. Effect of EPA and AA on delta-9 desaturase index. HepG2 cells with or without the core protein were incubated with EPA (A and C) or AA (B and D) for 48 h. The fatty acid compositions of the total cell lipids were analyzed and the ratios of 18:1/18:0 (A and B) and 16:1/16:0 (C and D) were computed. Light blue bars indicate control cells and dark blue bars indicate core-expressing cells. $N = 5$ in each group. $^{*}p < 0.05$. EPA, eicosapentaenoic acid; AA, arachidonic acid.

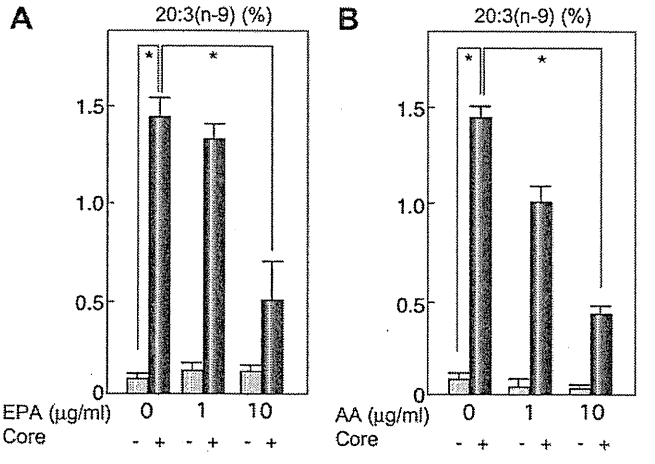

Fig. 4. Effect of EPA and AA on the concentration of 20:3(n-9). HepG2 cells with or without the core protein were incubated with EPA (A) or AA (B) for 48 h. The fatty acid compositions of the total cell lipids were analyzed and the percentages of the C20:3(n-9) fraction were measured. Light blue bars indicate control cells and dark blue bars indicate core-expressing cells. $N = 5$ in each group. $^{*}p < 0.05$.

suggested to be associated with HCV infection by the action of the HCV core protein [32–35]. Then, we explored the possibility that an increase in the NADH level, which is caused by the mitochondrial ETS dysfunction, induces the activation of fatty acid desaturases. Because fatty acid synthesis or fatty acid desaturation is accompanied by the oxidation of NAD(P)H, we measured the ketone body ratio (KBR) in the culture medium to estimate the redox state in the HepG2 cells expressing the core protein.

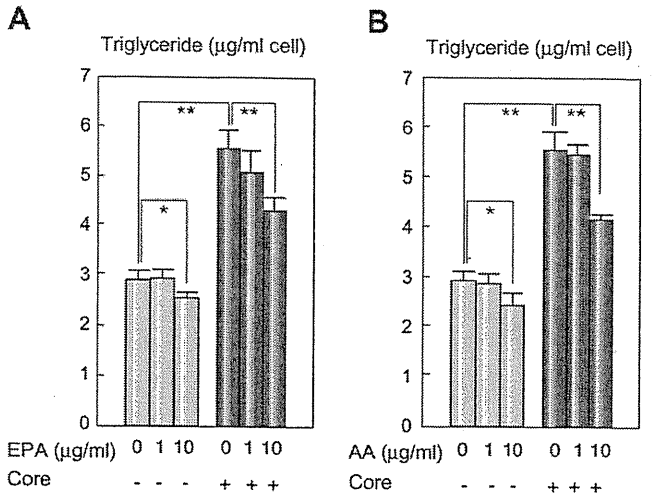

Fig. 5. Effect of EPA and AA on triglyceride content. HepG2 cells with or without the core protein were incubated with EPA (A) or AA (B) for 48 h. The triglyceride volume of the total cell lipids was measured and the triglyceride contents in the cells were calculated. Light blue bars indicate control cells and dark blue bars indicate core-expressing cells. $N = 5$ in each group. $^{*}p < 0.05$, $^{**}p < 0.01$.

The KBR, which is in equilibrium with the intramitochondrial $NAD^+/NADH$ [26,36], in the culture medium of the core-expressing cells, was significantly lower than that of control cells (Fig. 6A, $p < 0.01$). The ratio of lactate to pyruvate (lactate/pyruvate), which is proportional to the cytosolic $NADH/NAD^+$ [26], in the culture medium of the core-expressing cells was significantly higher than that of control cells (Fig. 6B, $p < 0.05$). These results, the higher $NADH/NAD^+$ ratio in both determinations, indicate that NADH accumulates in the core-expressing HepG2 cells, resulting in the overreduced state, as a consequence of the core protein expression. The amounts of total ketone bodies were significantly higher in the core-expressing cells than that in the control cells (Fig. 6C).

Effects of pyruvate on lipid metabolism in core-expressing cells

The addition of pyruvate into this constitutive core protein expression system, in which the pyruvate metabolism is in equilibrium, is expected to cause a reduction in the NADH level along with increases in the levels of lactate and NAD^+, because pyruvate tends to be converted to lactate by the action of lactate dehydrogenase (LDH) under the condition of high $NADH/NAD^+$ ratio [26,36]. Actually, the addition of pyruvate into the culture medium at various concentrations increased the KBR and reduced the amount of 5,8,11-eicosatrienoic acid (20:3 (n-9)) (Fig. 6D, $p < 0.05$ at 10 mM pyruvate), while it had no effect on the control cells. It also caused a reduction in the amount of triglyceride in the core-expressing cells but not in the control cells (Fig. 6E). This finding strongly supports the notion that NADH accumulation is, at least, one of the causes of the activation of fatty acid desaturases in this HCV model. The mRNA levels of anti-oxidant genes significantly decreased after the incubation with pyruvate at 10 mM (catalase, 1.27 ± 0.06 vs. 0.91 ± 0.05; glutathione synthetase 1.39 ± 0.04 vs. 1.01 ± 0.06; glutathione peroxidase 1.48 ± 0.03 vs. 1.23 ± 0.07, pyruvate (−) vs. pyruvate (+), $p < 0.05$, respectively), suggesting that pyruvate reduced the levels of oxidative stress in the core-expressing HepG2 cells.

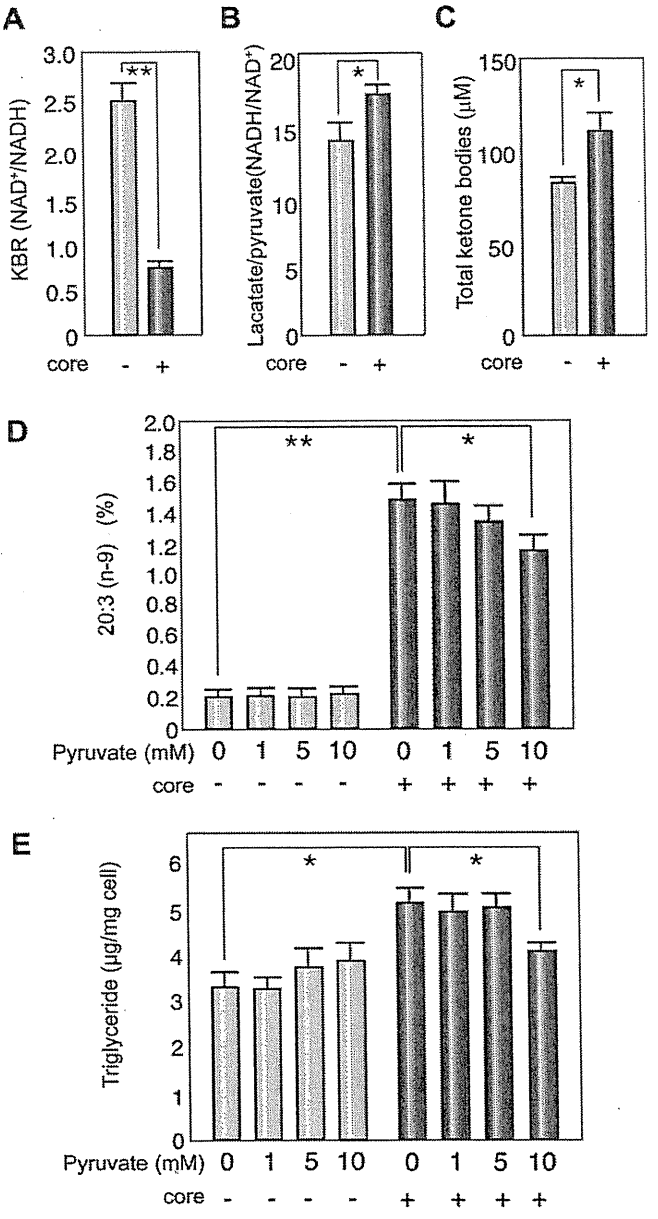

Fig. 6. NADH accumulation and effect of pyruvate in core-expressing cells. HepG2 cells with or without the core protein were subjected to the determination of ketone body ratio (A) and lactate/pyruvate ratio (B) for the precise estimation of NAD^+/NADH and NADH/NAD^+. (C) Total ketone bodies. (D) The percentages of the C20:3(n-9) fraction were measured after incubation with pyruvate at various concentrations. (E) The total amount of triglyceride was measured after incubation with pyruvate at various concentrations. Light blue bars indicate control cells and dark blue bars indicate core-expressing cells. $N = 5$ in each group. $^*p < 0.05$, $^{**}p < 0.01$.

Expression of SREBP-1 and desaturase genes in core-expressing cells

We previously showed that the core protein activates the expression of the SREBP-1c gene, which regulates the production of triglyceride [37] in the liver. We, therefore, examined the mRNA levels of genes associated with lipid metabolism in the current system. As shown in Fig. 7, the mRNA levels of SREBP-1c and delta-9 (stearoyl CoA) desaturase genes, but not that of the SREBP-1a gene, were significantly higher in the core-expressing cells than that in the control cells. Of note, the mRNA levels of the former two genes significantly decreased after the incubation with AA. The treatment with pyruvate also reduced the mRNA levels of the two genes, but the difference was not statistically significant compared with the control.

Discussion

The core protein of HCV modulated the activities of delta desaturases and changed the saturation states of fatty acids. The observed change in the HepG2 cells, namely, an increase in the amounts of unsaturated fatty acids, may support cell proliferation, by increasing the fluidity of the cell membrane as reported previously [20]. In the HepG2 cells expressing the core protein, the delta-6 desaturase activity was as high as that of the delta-9 desaturase, leading to the accumulation of a downstream product, 20:3(n-9) fatty acid. This was, unexpectedly, in contrast to our previous result on the liver tissues of HCV core gene transgenic mice, in which the 18:1/18:0 and 16:1/16:0 ratios were significantly higher than that in the liver tissues of normal littermate mice, indicating the activation of delta-9 desaturase [8]. The 16:1/16:0 and 18:1/18:0 ratios observed in the control HepG2 cells were consistent with the results of a previous study: the delta-6 desaturase activity is inherently higher in HepG2 cells than in normal mouse hepatocytes [28,29]. This may explain the difference in the effect of the core protein on lipid metabolism in these two systems, namely, HepG2 cells and mouse liver tissues. The significant increase in the delta-9 desaturase index and high concentration of 20:3(n-9) by the administration of ETYA, a delta-6 desaturase inhibitor, indicate the activation of delta-9 desaturase in the core-expressing cells. The results of real-time PCR analysis for determining the mRNA levels of these enzymes corroborated the current estimation of desaturase activities as determined by fatty acid analysis.

The mechanism underlying the activation of fatty acid desaturation by the HCV core protein is still unclear, but one possibility is the presence of an overreduced state in the core-expressing cells. The HCV core protein is closely associated with mitochondrial dysfunction, in particular, that of the respiratory chain complexes, resulting in an impairment of NADH oxidation [32–35]. NADH accumulation leads to an increase in desaturase activities through the augmentation of microsomal electron transfer [38]. In fact, the KBR in the core-expressing cells was significantly lower than that in the control cells, indicating the accumulation of NADH within the cells. The addition of pyruvate resulted in an increase in the KBR and a reduction in the amounts of triglyceride and 5,8,11-eicosatrienoic acid (20:3 (n-9)) while it had no effect on the control cells, strongly supporting the notion that NADH accumulation induced by the core protein is, at least, one of the causes of the activation of fatty acid desaturases in this HCV model.

Another possible mechanism underlying the accelerated desaturation is the activation of SREBP-1c, which controls the expression of delta-9 desaturase. In fact, the level of SREBP-1c mRNA was higher in the core-expressing cells than that in the control cells as reported previously [37]. The relief of NADH accumulation by pyruvate administration resulted in the reduced accumulation of triglyceride and unsaturated fatty acids, which was accompanied by the reduction in SREBP-1c and delta-9 desaturase gene expression levels. The intracellular accumulation of NADH might be involved in the activation of the SREBP-1c gene expression by the core protein. Thus, NADH accumulation, which

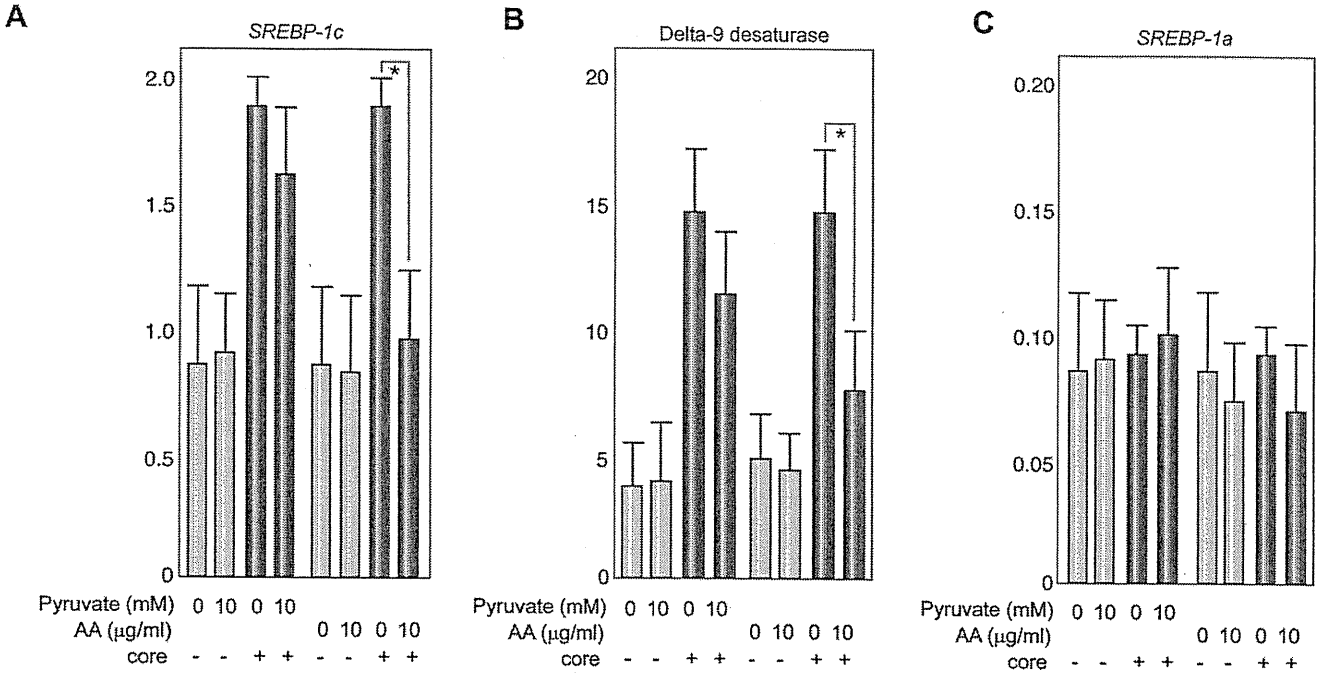

Fig. 7. Effect of pyruvate and AA on mRNA levels of lipid-associated genes. The mRNA levels of *SREBP-1c* (A), delta-9 desaturase (B) and *SREBP-1a* (C) genes were determined by real-time PCR analysis. The transcription of the genes was normalized with that of hypoxanthine phosphoribosyltransferase, and the values are expressed as relative activities. Light blue bars indicate control cells and dark blue bars indicate core-expressing cells. $N = 5$ in each group. $^*p < 0.05$. SREBP, sterol regulatory element binding protein.

is induced by the core protein through the impairment of the mitochondrial complex function [35], may be a key event that leads to the SREBP-1c activation, the desaturase activation, and the development of steatosis associated with HCV infection.

EPA and AA (PUFAs), which are known to suppress desaturase activities, lowered the 18:1/18:0 and 16:1/16:0 ratios and decreased the concentration of 20:3(n-9) concomitantly with that of triglyceride, regardless of the presence of the core protein, probably through SREBP-1c suppression (Fig. 7) [39]. On the other hand, the administration of EPA or AA did not affect the KBR in the core-expressing or control cells (data not shown), limiting the PUFAs ability to counteract the effect of the core protein. This is in contrast to the fact that the addition of pyruvate caused an increase in the KBR and a reduction in the amounts of triglyceride and 5,8,11-eicosatrienoic acid (20:3 (n-9)), while it had no effect on the control cells.

Fatty acid desaturation is closely associated with increased membrane fluidity [20], leading to augmented cell metabolism and higher cell division rates [21,22]. Although the relationship between carcinogenesis and lipid metabolism altered by the HCV core protein remains to be further clarified, alterations in lipid metabolism, in particular, in the desaturation of fatty acids, are closely associated with HCV infection, and PUFAs could prevent the pathogenesis of HCV-associated disorders involving lipid metabolism.

Conflict of interest

The authors who have taken part in this study declared that they do not have anything to disclose regarding funding or conflict of interest with respect to this manuscript.

Acknowledgments

This work was supported in part by Grant-in-Aid for Scientific Research on Priority Area from the Ministry of Education, Science, Sports, and Culture of Japan; Health Sciences Research Grants of The Ministry of Health, Labour, and Welfare (Research on Hepatitis); and a grant from The Sankyo Foundation of Life Science.

References

[1] Saito I, Miyamura T, Ohbayashi A, Harada H, Katayama T, Kikuchi S, et al. Hepatitis C virus infection is associated with the development of hepatocellular carcinoma. Proc Natl Acad Sci USA 1990;87:6547–6549.
[2] Schemer PJ, Ashrafzadeh P, Sherlock S, Brown D, Dusheiko GM. The pathology of chronic hepatitis C. Hepatology 1992;15:567–571.
[3] Bach N, Thung SN, Schaffner F. The histological features of chronic hepatitis C and autoimmune chronic hepatitis: a comparative analysis. Hepatology 1992;15:572–577.
[4] Fujie H, Yotsuyanagi H, Moriya K, Shintani Y, Tsutsumi T, Takayama T, et al. Steatosis and intrahepatic hepatitis C virus in chronic hepatitis. J Med Virol 1999;59:141–145.
[5] Moradpour D, Englert C, Wakita T, Wands JR. Characterization of cell lines allowing tightly regulated expression of hepatitis C virus core protein. Virology 1996;222:51–63.
[6] Barba G, Harper F, Harada T, Kohara M, Goulinet S, Matsuura Y, et al. Hepatitis C virus core protein shows a cytoplasmic localization and associates to cellular lipid storage droplets. Proc Natl Acad Sci USA 1997;94:1200–1205.
[7] Moriya K, Yotsuyanagi H, Shintani Y, Fujie H, Ishibashi K, Matsuura Y, et al. Hepatitis C virus core protein induces hepatic steatosis in transgenic mice. J Gen Virol 1997;78:1527–1531.
[8] Moriya K, Todoroki T, Tsutsumi T, Fujie H, Shintani Y, Miyoshi H, et al. Increase in the concentration of carbon 18 monosaturated fatty acids in the liver with hepatitis C: analysis in transgenic mice and humans. Biophys Biochem Res Commun 2001;281:1207–1212.
[9] Lerat H, Honda M, Beard MR, Loesch K, Sun J, Yang Y, et al. Steatosis and liver cancer in transgenic mice expressing the structural and nonstructural proteins of hepatitis C virus. Gastroenterology 2002;122:352–365.

[10] Naas T, Ghorbani M, Alvarez-Maya I, Lapner M, Kothary R, De Repentigny Y, et al. Characterization of liver histopathology in a transgenic mouse model expressing genotype 1a hepatitis C virus core and envelope proteins 1 and 2. J Gen Virol 2005;86:2185–2196.
[11] Adinolfi LE, Gambardella M, Andreana A, Tripodi MF, Utili R, Ruggiero G. Steatosis accelerates the progression of liver damage of chronic hepatitis C patients and correlates with specific HCV genotype and visceral obesity. Hepatology 2001;33:1358–1364.
[12] Massard J, Ratziu V, Thabut D, Moussalli J, Lebray P, Benhamou Y, et al. Natural history and predictors of disease severity in chronic hepatitis C. J Hepatol 2006;44:S19–S24.
[13] Leandro G, Mangia A, Hui J, Fabris P, Rubbia-Brandt L, Colloredo G, et al. HCV meta-analysis (on) individual patients' data study group. Relationship between steatosis, inflammation, and fibrosis in chronic hepatitis C: a meta-analysis of individual patient data. Gastroenterology 2006;130:1636–1642.
[14] Patton HM, Patel K, Behling C, Bylund D, Blatt LM, Vallee M, et al. The impact of steatosis on disease progression and early and sustained treatment response in chronic hepatitis C patients. J Hepatol 2004;40: 484–490.
[15] Harrison SA, Brunt EM, Qazi RA, Oliver DA, Neuschwander-Tetri BA, Di Bisceglie AM, et al. Effect of significant histologic steatosis or steatohepatitis on response to antiviral therapy in patients with chronic hepatitis C. Clin Gastroenterol Hepatol 2005;3:604–609.
[16] Moriya K, Fujie H, Shintani Y, Yotsuyanagi H, Tsutsumi T, Ishibashi K, et al. The core protein of hepatitis C virus induces hepatocellular carcinoma in transgenic mice. Nat Med 1998;4:1065–1067.
[17] Koike K. Molecular basis of hepatitis C virus-associated hepatocarcinogenesis: lessons from animal model studies. Clin Gastroenterol Hepatol 2005;3:S132–S135.
[18] Shi ST, Lee KJ, Aizaki H, Hwang SB, Lai MM. Hepatitis C virus RNA replication occurs on a detergent-resistant membrane that cofractionates with caveolin-2. J Virol 2003;77:4160–4168.
[19] Miyanari Y, Atsuzawa K, Usuda N, Watashi K, Hishiki T, Zayas M, et al. The lipid droplet is an important organelle for hepatitis C virus production. Nat Cell Biol 2007;9:1089–1097.
[20] Stubbs CD, Smith AD. The modification of mammalian membrane polyunsaturated fatty acid composition in relation to membrane fluidity and function. Biochim Biophys Acta 1984;779:89–137.
[21] Li J, Ding SF, Habib NA, Fermor BF, Wood CB, Gilmour RS. Partial characterization of a cDNA for human stearoyl-CoA desaturase and changes in its mRNA expression in some normal and malignant tissues. Int J Cancer 1994;57:348–352.
[22] Vinciguerra M, Carrozzino F, Peyrou M, Carlone S, Montesano R, Benelli R, et al. Unsaturated fatty acids promote hepatoma proliferation and progression through downregulation of the tumor suppressor PTEN. J Hepatol 2009;50:1132–1141.
[23] Ntambi JM. Regulation of stearoyl-CoA desaturase by polyunsaturated fatty acids and cholesterol. J Lipid Res 1999;40:1549–1558.
[24] Ruggieri A, Murdolo M, Harada T, Miyamura T, Rapicetta M. Cell cycle perturbation in a human hepatoblastoma cell line constitutively expressing hepatitis C virus core protein. Arch Virol 2004;149:61–74.
[25] Morrison WR, Smith LM. Preparation of fatty acid methyl esters and dimethylacetals from lipids with boron fluoride–methanol. J Lipid Res 1964;5:600–608.
[26] Williamson DH, Mellanby J, Krebs HA. Enzymic determination of D(-)-beta-hydroxybutyric acid and acetoacetic acid in blood. Biochem J 1962;82:90–96.
[27] Abid K, Pazienza V, Gottardi A, Rubbia-Brandt L, Conne B, Pugnale P, et al. An in vitro model of hepatitis C virus genotype 3a-associated triglycerides accumulation. J Hepatol 2005;42:744–751.
[28] Portolesi R, Powell BC, Gibson RA. Delta6 desaturase mRNA abundance in HepG2 cells is suppressed by unsaturated fatty acids. Lipids 2008;43:91–95.
[29] Choi Y, Park Y, Pariza MW, Ntambi JM. Regulation of stearoyl-CoA desaturase activity by the trans-10, cis-12 isomer of conjugated linoleic acid in HepG2 cells. Biochem Biophys Res Commun 2001;284:689–693.
[30] Strittmatter P, Spatz L, Corcoran D, Rogers MJ, Setlow B, Redline R. Purification and properties of rat liver microsomal stearyl coenzyme a desaturase. Proc Natl Acad Sci USA 1974;71:4565–4569.
[31] Joshi VC, Wilson AC, Wakil SJ. Assay for the terminal enzyme of the stearoyl coenzyme A desaturase system using chick embryo liver microsomes. J Lipid Res 1977;18:32–36.
[32] Korenaga M, Wang T, Li Y, Showalter LA, Chan T, Sun J, et al. Hepatitis C virus core protein inhibits mitochondrial electron transport and increases reactive oxygen species (ROS) production. J Biol Chem 2005;280: 37481–37488.
[33] Piccoli C, Scrima R, Quarato G, D'Aprile A, Ripoli M, Lecce L, et al. Hepatitis C virus protein expression causes calcium-mediated mitochondrial bioenergetic dysfunction and nitro-oxidative stress. Hepatology 2007;46:58–65.
[34] Tsutsumi T, Matsuda M, Aizaki H, Moriya K, Miyoshi H, Fujie H, et al. Proteomics analysis of mitochondrial proteins reveals overexpression of a mitochondrial protein chaperone, prohibitin, in cells expressing hepatitis C virus core protein. Hepatology 2009;50:378–386.
[35] Moriya K, Miyoshi H, Tsutsumi T, Shinzawa S, Fujie H, Shintani Y, et al. Tacrolimus ameliorates metabolic disturbance and oxidative stress caused by hepatitis C virus core protein: Analysis using mouse model and cultured cells. Am J Pathol 2009;175:1515–1524.
[36] Williamson DH, Lund P, Krebs HA. The redox state of free nicotinamide-adenine dinucleotide in the cytoplasm and mitochondria of rat liver. Biochem J 1967;103:514–527.
[37] Moriishi K, Mochizuki R, Moriya K, Miyamoto H, Mori Y, Abe T, et al. Critical role of PA28gamma in hepatitis C virus-associated steatogenesis and hepatocarcinogenesis. Proc Natl Acad Sci USA 2007;104:1661–1666.
[38] Jansson I, Schenkman JB. Studies on three microsomal electron transfer enzyme systems. Specificity of electron flow pathways. Arch Biochem Biophys 1977;178:89–107.
[39] Sekiya M, Yahagi N, Matsuzaka T, Najima Y, Nakakuki M, Nagai R, et al. Polyunsaturated fatty acids ameliorate hepatic steatosis in obese mice by SREBP-1 suppression. Hepatology 2003;38:1529–1539.

Clin Chem Lab Med 2011;49(4):751–752 © 2011 by Walter de Gruyter • Berlin • New York. DOI 10.1515/CCLM.2011.103

Letter to the Editor

Evaluation of multiplex PCR using dual-priming oligonucleotide for the detection of *vanA* and *vanB* in vancomycin-resistant enterococci

Ran Nagai[1,2], Ryoichi Saito[2,*], Saho Koyano[1,2], Noboru Okamura[2], Hiromitsu Yokota[3], Takatoshi Kitazawa[1] and Kyoji Moriya[1]

[1] Department of Infection Control and Prevention, The University of Tokyo Hospital, Tokyo, Japan
[2] Microbiology and Immunology, Department of Moleculo-Genetic Sciences, Graduate School of Health Care Sciences, Tokyo Medical and Dental University, Tokyo, Japan
[3] Department of Clinical Laboratory, The University of Tokyo Hospital, Tokyo, Japan

Keywords: dual-priming oligonucleotide; multiplex PCR; *vanA*; *vanB*.

Vancomycin-resistant enterococci (VRE) are multi-drug resistant pathogens that may cause serious nosocomial infections. Among the vancomycin resistance (Van) genes, *vanA* and *vanB* remain the most clinically relevant as they are associated with transposons and may mediate horizontal transfer of vancomycin resistance to other bacteria (1). Therefore, early detection of VRE is crucial for the management and treatment of both colonized and infected patients, and for appropriate implementation of infection control measures to prevent the spread of VRE. Until now, since PCR methods for detecting and identifying VRE are not cost-effective, a number of studies have attempted to develop and evaluate multiplex PCR for screening for VRE (2, 3). Generally, the results have shown that multiplex PCR is quicker and has higher sensitivity compared with conventional culture for the detection of *vanA* and *vanB*.

Recently, the Seeplex VRE detection assay (S-VRE; Seegene Inc., Seoul, Korea), based on a multiplex PCR using a dual-priming oligonucleotide (DPO) system, has been introduced. The DPO system is a new molecular technique for PCR, which contains two separate priming regions joined by a polydeoxyinosine linker. These primers allow a wide range of annealing temperatures and provide high sensitivity and specificity which helps prevent false-positive results (4–6). In this study, we evaluated the performance of S-VRE for the simultaneous detection of *vanA* and *vanB* in VRE.

Five VRE strains [three *Enterococcus faecium* isolated in a clinical laboratory (*vanA*), one *Enterococcus faecalis* ATCC51299 (*vanB*) and one *Enterococcus casseliflavus* isolated in a clinical laboratory (*vanC-2*)] and *E. faecalis* ATCC 29212 were used as glycopeptide resistant controls and a wild type control, respectively. To determine the analytical sensitivity of the S-VRE, DNA templates were obtained from the supernatant of boiled extracts of a clinical isolate of *E. faecium* carrying *vanA* and *E. faecalis* V583 carrying *vanB* harvested from a trypticase soy agar plate with 5% defibrinated sheep blood (Nissui Pharmaceutical, Tokyo, Japan). Their concentrations were measured using a spectrophotometer (Thermo Fisher Scientific, Wilmington, DE, USA). The number of genomic copies for S-VRE was calculated by assuming the molecular size of *E. faecalis* V583 to be 3.21 Mbp (GenBank accession no. NC_004668). The amplification profile of this assay is as follows: initial denaturation at 94°C for 15 min, 35 cycles of amplification (denaturation at 94°C for 30 s, annealing at 60°C for 1 min, and extension at 72°C at 1 min), and final extension at 72°C for 10 min. Amplification was performed using a thermal cycler (Applied Biosystems, Foster City, CA, USA). Also, multiplex PCR amplification of *vanA* and *vanB* was performed using primer sets according to a method described previously [K-PCR; 3]. Amplified PCR products were separated by electrophoresis in 2.0% agarose and visualized by ethidium bromide staining. Each assay was performed three times to check for variation. For clinical evaluation, a total of 50 stool specimens collected from hospitalized patients between May and June 2009 were included in this study and analyzed in singlicate. Stool specimens for culture were directly inoculated onto VRE agar plates (Becton Dickinson, Tokyo, Japan) containing 6 mg/L vancomycin. All isolates growing on VRE agar plates were regarded as presumptive VRE and identified using the VITEK Legacy system (Sysmex-bioMerieux, Tokyo, Japan).

The minimum concentrations of *vanA* and *vanB* detected by S-VRE were 2.5 and 8.5×10^2 copies/reaction, respectively (Figure 1). Similarly, those detected by K-PCR were 2.5×10^3 and 8.5×10^3 copies/reaction, respectively. Compared to K-PCR, S-VRE of *vanA* and *vanB* had 1.0×10^3

*Corresponding author: Ryoichi Saito, PhD, Microbiology and Immunology, Department of Moleculo-Genetic Sciences, Graduate School of Health Care Sciences, Tokyo Medical and Dental University, 1-5-45 Yushima, Bunkyo-ku, Tokyo 113-8510, Japan. Phone/Fax: +81-3-5803-5375, E-mail: saito-lab@umin.ac.jp
Previously published online January 31, 2011

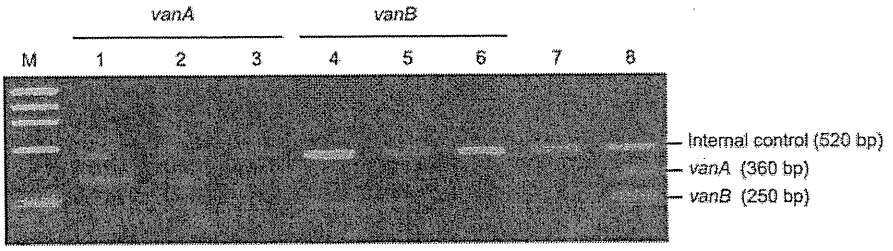

Figure 1 Analytical sensitivity of the Seeplex VRE detection assay for the detection of *vanA* and *vanB* in enterococcal isolates using serial dilutions of the DNA template.
Lane M, φ×174/*Hae*III; lanes 1, 2, 3, 4, 5, and 6, 2.5×10^1, 2.5, 0.25, 8.5×10^3, 8.5×10^2 and 8.5×10^1 copies/reaction, respectively; lane 7, the template DNA of a glycopeptide-susceptible *E. faecalis*; lane 8, VRE size marker.

and 10-fold higher sensitivity, respectively. For clinical evaluation, none of the isolates growing on VRE agar plates was positive for *vanA* and/or *vanB* by S-VRE and K-PCR. However, the sensitivity of S-VRE applied to stool specimens with varying densities of *vanA*- or *vanB*-positive isolates was 10^3 cfu/g stool (*vanA*) and 10^4 cfu/g stool (*vanB*).

In this study, S-VRE was considerably more sensitive and easy to perform compared with K-PCR for detecting the Van genes. Furthermore, S-VRE can check the presence of PCR inhibitors since it contains an internal control. These results were similar to previous findings that DPO-based multiplex PCR was a useful diagnostic method (4–6). Moreover, D'Agata et al. (7) demonstrated that the mean density of VRE was 6 ± 2 $\log_{10}$ cfu/g stool in patients with VRE colonization or infection. Therefore, we have demonstrated that S-VRE offers detection of VRE directly from colonies growing on VRE agar plates within a few hours, with high sensitivity, and can help with the rapid deployment of infection control and prevention measures.

One limitation of this study is the small number of VRE isolates. However, our study indicates that S-VRE represents a significant improvement over the previous method of multiplex PCR for detection of *vanA* and *vanB*.

Conflict of interest statement

Authors' conflict of interest disclosure: The authors stated that there are no conflicts of interest regarding the publication of this article.

Research funding: None declared.
Employment or leadership: None declared.
Honorarium: None declared.

References

1. Gold HS. Vancomycin resistant enterococci: mechanism and clinical observations. Clin Infect Dis 2001;33:210–21.
2. Patel R, Uhl JR, Kohner P, Hopkins MK, Cockerill FR 3rd. Multiplex PCR detection of vanA, vanB, vanC-1, and vanC-2/3 genes in enterococci. J Clin Microbiol 1997;35:703–7.
3. Kariyama R, Mitsuhata R, Chow JW, Clewell DB, Kumon H. Simple and reliable multiplex PCR assay for surveillance isolates of vancomycin-resistant enterococci. J Clin Microbiol 2000;38: 3092–5.
4. Chun JY, Kim KJ, Hwang IT, Kim YJ, Lee DH, Lee IK, et al. Dual priming oligonucleotide system for the multiplex detection of respiratory viruses and SNP genotyping of CYP2C19 gene. Nucleic Acids Res 2007;35:e40.
5. Horii T, Ohtsuka H, Osaki M, Ohkuni H. Use of a dual priming oligonucleotide system to detect multiple sexually transmitted pathogens in clinical specimens. Lett Appl Microbiol 2009;49: 46–52.
6. Drews SJ, Eshaghi A, Pyskir D, Chedore P, Lombos E, Broukhanski G, et al. The relative test performance characteristics of two commercial assays for the detection of Mycobacterium tuberculosis complex in paraffin-fixed human biopsy specimens. Diagn Pathol 2008;3:37.
7. D'Agata EM, Gautam S, Green WK, Tang YW. High rate of false-negative results of the rectal swab culture method in detection of gastrointestinal colonization with vancomycin-resistant enterococci. Clin Infect Dis 2002;34:167–72.

Antiviral Therapy 2012; 17:35–43 (doi: 10.3851/IMP1923)

Original article

Age and total ribavirin dose are independent predictors of relapse after interferon therapy in chronic hepatitis C revealed by data mining analysis

*Masayuki Kurosaki[1], Naoki Hiramatsu[2], Minoru Sakamoto[3], Yoshiyuki Suzuki[4], Manabu Iwasaki[5], Akihiro Tamori[6], Kentaro Matsuura[7], Sei Kakinuma[8], Fuminaka Sugauchi[9], Naoya Sakamoto[8], Mina Nakagawa[8], Hiroshi Yatsuhashi[10], Namiki Izumi[1]**

[1]Division of Gastroenterology and Hepatology, Musashino Red Cross Hospital, Tokyo, Japan
[2]Department of Gastroenterology and Hepatology, Osaka University Graduate School of Medicine, Osaka, Japan
[3]First Department of Internal Medicine, University of Yamanashi, Yamanashi, Japan
[4]Department of Hepatology, Toranomon Hospital, Tokyo, Japan
[5]Department of Computer and Information Science, Seikei University, Tokyo, Japan
[6]Department of Hepatology, Osaka City University Medical School, Osaka, Japan
[7]Department of Gastroenterology and Metabolism, Nagoya City University Graduate School of Medical Sciences, Nagoya, Japan
[8]Department of Gastroenterology and Hepatology, Tokyo Medical and Dental University, Tokyo, Japan
[9]Department of Gastroenterology, Nagoya Koseiin Medical Welfare Center, Nagoya, Japan
[10]Clinical Research Center, National Nagasaki Medical Center, Nagasaki, Japan

*Corresponding author e-mail: nizumi@musashino.jrc.or.jp

Background: This study aimed to define factors associated with relapse among responders to pegylated interferon (PEG-IFN) plus ribavirin (RBV) therapy in chronic hepatitis C.

Methods: A cohort of genotype 1b chronic hepatitis C patients treated with PEG-IFN plus RBV and who had an undetectable HCV RNA by week 12 (n=951) were randomly assigned to model derivation (n=636) or internal validation (n=315) groups. An independent cohort (n=598) were used for an external validation. A decision tree model for relapse was explored using data mining analysis.

Results: The data mining analysis defined five subgroups of patients with variable rates of relapse ranging from 13% to 52%. The reproducibility of the model was confirmed by internal and external validations (r^2=0.79 and 0.83, respectively). Patients with undetectable HCV RNA at week 4 had the lowest risk of relapse (13%), followed by patients <60 years with undetectable HCV RNA at week 5–12 who received ≥3.0 g/kg of body weight of RBV (16%). Older patients with a total RBV dose <3.0 g/kg had the highest risk of relapse (52%). Higher RBV dose beyond 3.0 g/kg was associated with further decrease of relapse rate among patients <60 years (up to 11%) but not among older patients whose relapse rate remained stable around 30%.

Conclusions: Data mining analysis revealed that time to HCV RNA negativity, age and total RBV dose was associated with relapse. To prevent relapse, ≥3.0 g/kg of RBV should be administered. Higher dose of RBV may be beneficial in patients <60 years.

Introduction

The currently recommended therapy for chronic hepatitis C is a combination of pegylated interferon (PEG-IFN) plus ribavirin (RBV) [1]. This therapy is effective in 50% of patients with HCV genotype 1b [2,3]. The most reliable predictor of sustained virological response (SVR) is the response during early weeks of therapy. A satisfactory response to therapy in the early weeks is associated with a high rate of SVR [4–8]. A basic concept of response-guided therapy is to modify the duration of therapy according to the time to HCV RNA negativity. Extended therapy may be given to patients with delayed virological response [9–13]. Modification of duration of therapy or drug dose may also be necessary in patients with early virological

response (EVR), because approximately 20% of these patients experience relapse after the completion of 48 weeks of therapy. Recent reports have revealed that single nucleotide polymorphisms located near the *IL28B* gene are strongly associated with SVR or a null response to PEG-IFN plus RBV therapy [14–16]. However, single nucleotide polymorphisms located near the *IL28B* gene are not associated with relapse after EVR [17]. Identification of risk factors for relapse among patients with virological response may lead to more individualized therapy and improved SVR rate.

Decision tree analysis, a core component of data mining analysis, is a method that explores data to develop predictive models [18]. This method has been originally used in business and recently in medical fields [19–25]. Decision tree analysis was successfully used to build a predictive model of EVR [26] and SVR to PEG-IFN plus RBV combination therapy in chronic hepatitis C [17,27,28]. The results of the analysis are presented as a tree structure, which is easy to understand and use in clinical practice. Patients can be allocated into subgroups by simply following the flowchart form of the decision tree [29].

In the present study, we used decision tree analysis to identify predictors of relapse among patients who achieved EVR to PEG-IFN plus RBV therapy, and to define a more individualized therapeutic strategy beyond response-guided therapy.

Table 1. Background of study population

Characteristic	Value
Age, years	54.9 (10.8)
Gender	–
Male, *n* (%)	557 (59)
Female, *n* (%)	394 (41)
Body mass index, kg/m^2	23.2 (3.3)
Albumin, g/dl	4.1 (1.8)
Creatinine, mg/dl	0.7 (0.2)
AST, IU/l	60.6 (46.2)
ALT, IU/l	80.7 (77.2)
GGT, IU/l	52.0 (60.0)
White blood cell count, cells/μl	4,993 (1,363)
Haemoglobin, g/dl	15.9 (52.6)
Platelets, 10^9/l	174.4 (6.1)
HCV RNA, KIU/ml	1,655 (1,455)
Fibrosis stage	–
F1-2, *n* (%)	626 (66)
F3-4, *n* (%)	98 (10)
NA, *n* (%)	227 (24)
Time to HCV RNA negativity 4/8/12 weeks	–
4 Weeks, *n* (%)	233 (24)
8 Weeks, *n* (%)	386 (41)
12 Weeks, *n* (%)	332 (35)
Treatment duration, weeks	42 (13)
Total RBV dose, g/kg body weight	3.1 (1.3)
Total PEG-IFN dose, μg/kg body weight	62.5 (38.6)
Outcome	–
Relapse, *n* (%)	238 (25)
SVR, *n* (%)	713 (75)

Total *n*=951. Data are expressed as mean (SD) unless otherwise indicated. ALT, alanine aminotransferase; AST, aspartate aminotransferase; GGT, γ-glutamyltransferase; NA, not available; PEG-IFN, pegylated interferon; RBV, ribavirin; SVR: sustained virological response.

Methods

Patients

This is a multicentre retrospective cohort study involving Musashino Red Cross Hospital, Toranomon Hospital, Tokyo Medical and Dental University, Osaka University, Nagoya City University, Yamanashi University, Osaka City University, and their related hospitals. The inclusion criteria were chronic hepatitis C patients treated with PEG-IFN-α2b plus RBV, genotype 1b, pretreatment HCV RNA titre >100 KIU/ml as confirmed by quantitative PCR; Cobas Amplicor HCV Monitor version 2.0; Roche Diagnostic Systems, Pleasanton, CA, USA), an undetectable HCV RNA level within week 12 after the start of therapy, no coinfection with HBV or HIV, and no other causes of liver disease. Patients were treated with PEG-IFN-α2b (1.5 μg/kg) subcutaneously every week plus a daily weight-adjusted RBV dose (600 mg for patients weighing <60 kg, 800 mg for patients weighing 60–80 kg and 1,000 mg for patients weighing >80 kg). Dose reduction or discontinuation of PEG-IFN and RBV was considered based on the recommendations of the package inserts and the discretion of physicians at each university and hospital. The standard duration of therapy was set at 48 weeks, but extension of duration was allowed and implemented at the discretion of each physician. The duration of therapy was extended beyond 48 weeks in 118 patients (mean duration was 56.3 weeks, ranging from 49 to 72 weeks). Although the exact reason for the prolonged treatment in each case was not available, one reason may be that each physician tried to achieve high adherence of RBV by extending the duration of therapy. Another reason may be the late time point of HCV RNA negativity even within early virological response. Among 118 patients, time to HCV RNA negativity was between 9 to 12 weeks in 56% of patients.

A total of 951 patients fulfilled the study criteria. The baseline characteristics and representative laboratory test results are listed in Table 1. For analysis, patients were randomly assigned to either the model derivation (636 patients) or internal validation (315 patients) groups. There were no significant differences in the clinical backgrounds between these two groups. For external validation of the model, we collaborated with another multicentre study group consisting of 29 medical centres and hospitals belonging to the National

Hospital Organization (Japan). A dataset collected from 598 patients who were treated with PEG-IFN-α2b plus RBV and had undetectable HCV RNA within week 12 were used for external validation. Informed consent was obtained from each patient. The study protocol conformed to the ethical guidelines of the Declaration of Helsinki and was approved by the institutional review committees of all concerned hospitals.

Laboratory tests

Haematological tests, blood chemistry and HCV RNA titre were analysed before therapy and at least once every month during therapy. Rapid virological response (RVR) was defined as an undetectable HCV RNA level at week 4, and complete early virological response (cEVR) was defined as an undetectable HCV RNA level at week 5 through week 12 after the start of therapy. SVR was defined as an undetectable HCV RNA level 24 weeks after the completion of therapy. Detection of HCV RNA level was based on qualitative PCR with a lower detection limit of 50 IU/ml (Amplicor; Roche Diagnostic Systems). A database of pretreatment variables included haematological tests (haemoglobin level, white blood cell count and platelet count), blood chemistry tests (serum levels of creatinine, albumin, aspartate aminotransferase, alanine aminotransferase, γ-glutamyltransferase, total cholesterol, triglycerides and HCV RNA titre), stage of histological fibrosis and patient characteristics (age, sex and body mass index). Post-treatment variables included time to HCV RNA negativity, calculated total RBV dose (g/kg of body weight), and calculated total PEG-IFN dose (μg/kg of body weight).

Statistical analysis

The Student's *t*-test was used for the univariable comparison of quantitative variables and Fisher's exact test was used for the comparison of qualitative variables. Logistic regression models with backward selection procedures were used for multivariable analysis of factors associated with relapse. IBM SPSS software version 18.0 (SPSS Inc., Chicago, IL, USA) was used for analysis. For the decision tree analysis [30], the data mining software IBM SPSS Modeler 14 (SPSS Inc.) was used, as reported previously [17,26–28]. The decision tree analysis, the core component of the data mining, belongs to a family of non-parametric regression methods based on binary recursive partitioning of data. In this analysis, the software automatically explored the database to determine optimal split variables to build a decision tree structure. A statistical search algorithm evaluate the model derivation group to determine the optimum variables and cutoff values and to yield the most significant division of patients into two subgroups that were as homogeneous as possible for the probability of relapse. Once patients were divided into 2 subgroups, the analysis was automatically repeated on each subgroup in the same way until either no additional significant variable was detected or the number of patients was <20. Finally all patients were classified into particular subgroups that are homogeneous with respect to the probabilities of relapse.

Results

The decision tree model for the prediction of relapse

The overall rate of relapse was 26% in the model derivation group. The decision tree analysis selected three variables that are associated with relapse: time to HCV RNA negativity, age and total RBV dose (Figure 1). Time to HCV RNA negativity was selected as the best predictor of relapse. The rate of relapse was 13% for patients with RVR compared to 30% for patients with cEVR. Among patients with cEVR, age was selected as the variable of second split. Patients <60 years had a lower probability of relapse (22%) compared with those ≥60 years (41%). The total RBV dose was selected as the third variable of split with an optimal cutoff of 3.0 g/kg of body weight. The rate of relapse was lower in patients who received ≥3.0 g/kg of body weight of RBV compared to patients who received <3.0 g/kg of body weight (among patients <60 years rates were 16% versus 32% and among patients ≥60 years rates were 26% versus 52%, respectively).

According to this decision tree, the patients were divided into five groups with different rates of relapse ranging from 13% to 52%. Patients with RVR had the lowest risk of relapse. Among patients with cEVR, patients <60 years who received ≥3.0 g/kg of body weight of RBV also had a low risk of relapse (16%). By contrast, patients who received <3.0 g/kg of body weight of RBV had higher than the average risk of relapse, especially in patients ≥60 years (52%).

Validation of the decision tree model

The decision tree model was validated using an internal validation group that was not included in the model derivation. The rates of relapse for each subgroup of patients were correlated closely between the model derivation and the internal validation group (r^2=0.79; Figure 2A). When validated using an external validation group, the rates of relapse for each subgroup of patients were again correlated closely between the model derivation and the external validation group. (r^2=0.83; Figure 2B).

Multivariable logistic regression analysis for factors associated with relapse

Univariable and multivariable analysis was performed using the combined population of model derivation and internal validation group. Univariable analysis found

that age, sex, serum levels of creatinine, haemoglobin, platelet count, HCV RNA titre, time to HCV RNA negativity, total PEG-IFN dose and total RBV dose were associated with relapse. Duration of therapy was not associated with reduction in relapse rate. Multivariable analysis including these factors showed that age, total RBV dose, serum level of creatinine, and time to HCV RNA negativity were independent predictors of relapse (Table 2). Creatinine was not selected as a splitting variable in data mining analysis probably due to the limitation to stop the analysis when the number of patients was <20. Using the combined population of model derivation and internal validation group, patients in each subgroup of decision tree model were further stratified by creatinine levels and the effect of creatinine level on relapse was analysed. Among patients with RVR, the rate of relapse did not differ between patients with creatinine levels of <0.7 g/dl and ≥0.7 g/dl and were 12% and 12%, respectively. Among patients with cEVR, the rate of relapse was higher in patients with creatinine levels of <0.7 g/dl compared to those with creatinine levels of ≥0.7 g/dl and were 39% versus 23%, respectively, for patients <60 years who received <3.0 g/kg of body weight of RBV, 19% versus 14% for patients <60 years who received ≥3.0 g/kg of body weight of RBV, 58% versus 41% for patients ≥60 years who received <3.0 g/kg of body weight of RBV, and 42% versus 26% for patients ≥60 years who received ≥3.0 g/kg of body weight of RBV.

Effect of age and total RBV dose on relapse among patients with cEVR

The effect of total RBV dose on relapse was analysed among patients with cEVR in a combined group of

Figure 1. The decision-tree model of relapse among patients with rapid virological response or complete early virological response

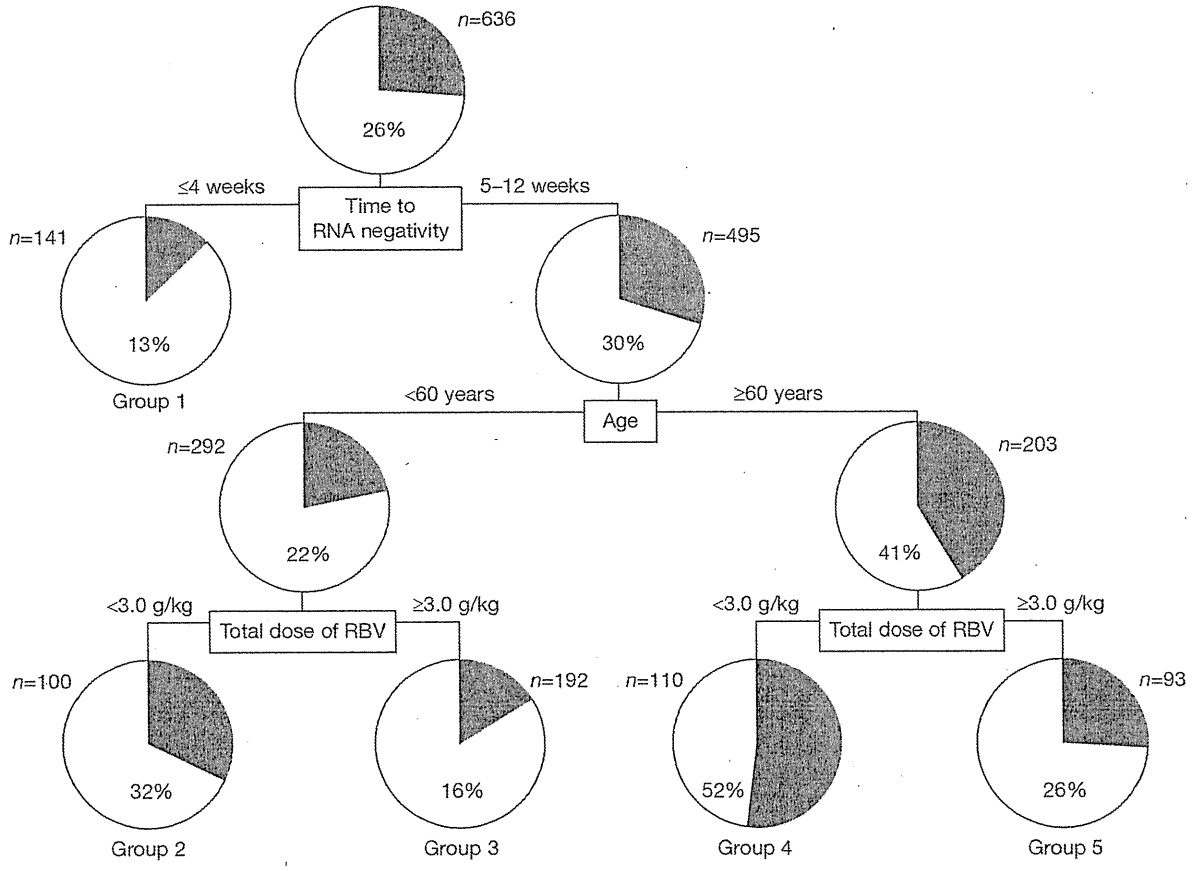

Boxes indicate the factors used for splitting and the cutoff values for the split. Pie charts indicate the rate of relapse for each group of patients after splitting. Terminal groups of patients discriminated by the analysis are numbered from 1 to 5. The rate of relapse was higher than average (>26%) in subgroups 2 and 4, where total ribavirin (RBV) dose was <3 g/kg of body weight.

model derivation and internal validation (n=718). The relapse rate decreased with an increase in RBV dose (Figure 3A). When patients were stratified into two groups according to age, the relapse rate decreased with an increase in RBV dose in patients <60 years. The relapse rate was lowest (11%) in patients <60 years who received ≥4.0 g/kg of body weight of RBV. By contrast, among patients ≥60 years, the relapse rate decreased with an increase in RBV dose up to 3.0 g/kg of body weight, but remained relatively stable despite a further increase in the RBV dose beyond 3.0 g/kg of body weight. The rate of relapse was 31% to 33% in patients who received ≥3.0 g/kg of body weight. Patients ≥60 years had higher relapse rate compared with patients <60 years after stratification by RBV dose (P=0.044 for RBV <2.5 g/kg, P=0.009 for RBV 2.5–2.9 g/kg, P=0.150 for RBV 3.0–3.4 g/kg, P=0.036 for RBV 3.5–3.9 g/kg and P=0.006 for RBV ≥4.0 g/kg).

To exclude the effect of the duration of therapy, patients who received 42–54 weeks of therapy were selected (n=544). Again, the relapse rate decreased with an increase in RBV dose in patients <60 years but remained stable despite a further increase in the RBV dose beyond 3.0 g/kg of body weight in patients ≥60 years (Figure 3B); in addition, patients ≥60 years had a higher relapse rate compared with younger patients after stratification by

Figure 2. Internal and external validation of the decision-tree model: subgroup-stratified comparison of the rate of relapse between the model derivation and validation groups

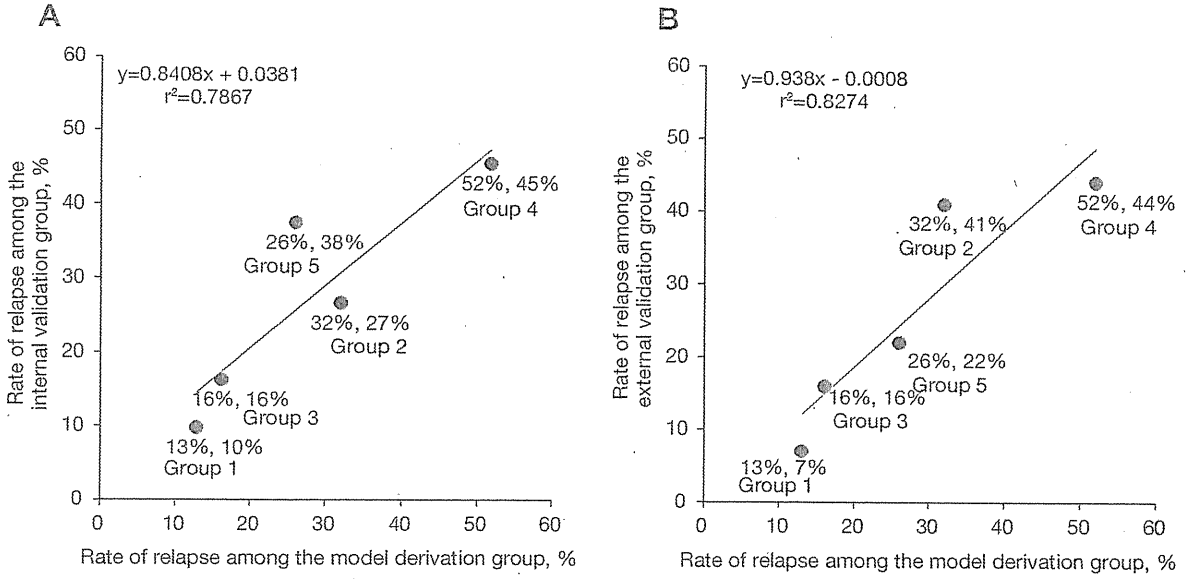

Each patient in the internal and external validation population was allocated to groups 1 to 5 following the flowchart of the decision tree. The rates of relapse were then calculated for each group and a graph was plotted. The rate of relapse in the (A) internal and (B) external validation groups are shown. The rates of relapse are shown as percentages below data points: the value on the left is from the model derivation group and on the right is from the validation group. The rates of relapse in each group of patients correlated closely between the model derivation group and the validation group (correlation coefficient: r^2=0.79 and 0.83, respectively).

Table 2. Multivariable analysis of factors associated with relapse among patients with RVR/cEVR

Factor	OR	95% CI	P-value
No-RVR	4.07	2.57–6.43	<0.0001
Total RBV dose <3.0 g/kg body weight	2.19	1.58 –3.03	<0.0001
Creatinine <0.7 g/dl	1.67	1.22–2.29	0.001
Age ≥60 years	2.37	1.73–3.24	<0.0001

cEVR, complete early virological response (HCV-RNA-positive at week 4, but negative at week 12); RBV, ribavirin; RVR, rapid virological response (HCV-RNA-negative at week 4).

RBV dose (P=0.283 for RBV <2.5 g/kg, P=0.017 for RBV 2.5–2.9 g/kg, P=0.127 for RBV 3.0–3.4 g/kg, P=0.011 for RBV 3.5–3.9 g/kg and P=0.009 for RBV ≥4.0 g/kg).

Total dose of RBV was associated with relapse independently of PEG-IFN dose. The cutoff value of 58 zμg/kg of PEG-IFN was selected, which corresponds to the 80% of 1.5 μg/kg dose for 48 weeks. In patients who received <58 μg/kg of body weight of PEG-IFN, the rate of relapse for patients who received ≥3.0 g/kg or <3.0 g/kg of body weight of RBV was 24% and 42%, respectively. In patients who received ≥58 μg/kg of body weight of PEG-IFN, the rate of relapse for patients who received ≥3.0 g/kg or <3.0 g/kg of body weight of RBV was 21% and 38%, respectively.

The data mining analysis procedure did not select further split variables among RVR patients. However,

Figure 3. Correlation between the rate of relapse and total RBV dose among patients with cEVR after stratification by age

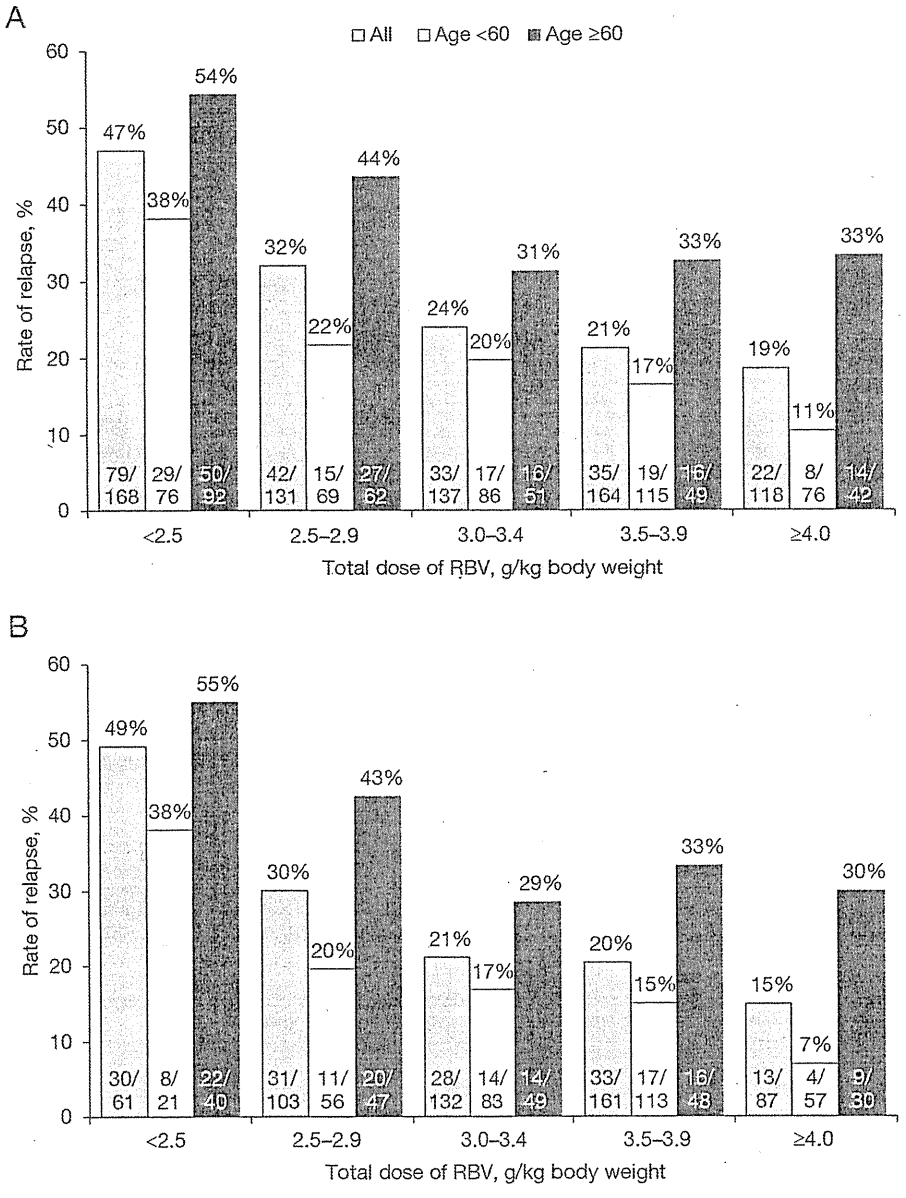

Association between the total ribavirin (RBV) dose and the rate of relapse among patients with complete early virological response (cEVR) is shown. (A) Higher dose of RBV was associated with reduced rate of relapse. (B) These associations were also confirmed in selected patients who received 42–54 weeks of therapy.